AMERICAN JOURNAL OF BIOCHEMISTRY AND BIOTECHNOLOGY

RESEARCH ARTICLE

Preparation and Properties Study of PCM@ECD Bilayer

Yan Zhao[1], Heng Zhang[1], Yanfei Zhao[1], Madiha Younas[1], Qingfeng Rong[2], Qing Shao[1], Lanlan Zhu[1]*

[1]School of Agricultural Engineering and Food Science, Shandong University of Technology, Zibo, China
[2]Zichuan District Inspection and Test Center, Zibo, Shandong Province, China

*Corresponding Author: chinaxiaolan@163.com

Abstract: This study reports the fabrication of a core-shell active bilayer membrane (PCM@ECD) via a combined tape-casting and layer-transfer methodology. The inner core layer comprised Pectin-Chitosan (PC) microcapsules, synthesized by complex coacervation, encapsulating Orange Peel Essential Oil (OPEOM) with an embedding efficiency of 83.08%. The outer shell layer consisted of Ethyl Cellulose (EC) doped with zinc-doped carbon dots (Zn-CDs, average size: 1.72 nm). The microencapsulation of OPEOM facilitated the sustained release of its active components, primarily limonene, and significantly enhanced its stability. The incorporated Zn-CDs conferred potent UV-shielding properties, attributed to π→π* and n→π* electronic transitions across the 200–400 nm wavelength range. Optimized at loadings of 15% (w/w) OPEOM and 0.01% (w/w) Zn-CDs, the composite bilayer film demonstrated superior functional performance: enhanced tensile strength (28.7 ± 1.2 MPa), a 38.2% reduction in water vapor permeability (WVP), exceptional UV-blocking efficacy (>95% at 350 nm), significant antibacterial activity (inhibition rates of 87.0% and 66.7% against *Shewanella putrefaciens* and *Pseudomonas* sp., respectively), and high antioxidant capacity (79.97% DPPH radical scavenging). This work pioneers a synergistic preservation strategy utilizing Zn-CDs and OPEO microcapsules, demonstrating significant potential for application in high-moisture food systems.

Keywords: Active Bilayer Film, Zinc-Doped Carbon Dots, Essential Oil Microcapsules, Controlled Release, Core-Shell

Received: 09-07-2025 | **Revised:** 26-08-2025 | **Accepted:** 07-10-2025 | **DOI:** 10.3844/ajbbsp.2026.22.01.006

Introduction

Salmon's rich nutrients, including high-quality protein, polyunsaturated fats, and astaxanthin, make it a popular worldwide [1]. However, its high moisture and nutrients make it susceptible to spoilage and microbial contamination, increasing the risk of deterioration and foodborne illnesses without proper preservation [2, 3]. The development of multifunctional properties such as antioxidant and antimicrobial activity in antimicrobial active packaging provides a promising solution [4]. For example, adding grape leaf carbon dots as an active ingredient to a dialdehyde persian gelatine-gelatin film increases antioxidant activity from 16.66% to 94.08%, the prepared film is non-cytotoxic, and the shelf life of trout fillets is prolonged by 4 days [5]. Edible chitosan-based films were prepared by loading chitosan/carrageenan capsules with red cabbage and clove bud oil as deterioration indicators and antibacterial agents, respectively. The results showed that the films had the potential to inhibit the growth of fish microorganisms and clearly indicated the freshness of fish [6].

Extensive research has attributed numerous therapeutic potentials to orange essential oil, encompassing antioxidant, anticancer, anti-inflammatory, cardioprotective, neuroprotective, antibacterial, and antifungal activities [7]. In orange, the essential oil is predominantly localized within the flavedo of the peel, with lesser quantities present in the leaves [8]. Consequently, Orange Peel Essential Oil (OPEO) was selected for this investigation to function as a natural antibacterial agent. A principal limitation to its application, however, is its inherent volatility and susceptibility to oxidative degradation, which can rapidly diminish its antimicrobial efficacy. To mitigate this instability, microencapsulation was employed. This established technology is widely utilized across the food, chemical, and pharmaceutical industries for the protection, stabilization, and controlled release of labile active compounds [9].

The microencapsulation of Orange Peel Essential Oil (OPEO) as a core material presents an effective strategy to mitigate its volatility and preserve its bioactive properties. This approach is supported by prior research; for instance, Jun-xia et al. demonstrated that microencapsulation of citrus oil within a matrix of soy protein isolate and gum arabic significantly enhanced the retention of its characteristic flavor compounds and d-limonene content [10]. The efficacy of this technique extends to other essential oils, as evidenced by Park et al. who fabricated clove bud oil-loaded capsules via an ionic gelation method using chitosan and carrageenan [6]. Their findings, confirmed by Minimum Inhibitory Concentration (MIC) assays and time-kill kinetic studies, revealed that films incorporated with these microcapsules exhibited superior antibacterial activity compared to those containing non-encapsulated oil [11]. Another study reported that a film embedded with cinnamaldehyde microcapsules sustained long-term antifungal activity. Beyond polysaccharide and protein-based wall materials, Maillard Reaction Products (MRPs) derived from whey protein isolate and various reducing sugars (e.g., glucose, fructose, maltose, lactose) have also been successfully employed. Microcapsules formulated with the optimal MRP significantly improved the oxidative stability of encapsulated tuna oil during storage [12].

Chitosan is a natural polymer with a variety of biological properties, found in the exoskeleton of crustaceans and insects [13]. Chitosan is a non-toxic, renewable, biodegradable, biocompatible GRAS biopolymer with excellent film-forming abilities. However, its high hydrophilicity and limited mechanical, barrier, and water-resistant properties restrict its use in food packaging [14]. To address these issues, its properties can be enhanced by creating bio-composites with other biopolymers like gelatin [15]. Pectin, a plant cell wall polysaccharide made of α-(1,4)-linked d-galacturonic acids, also has gel-forming properties [16] (Sharaby et al. 2022). It is nontoxic, water-soluble, negatively charged, biocompatible and biodegradable, making it an ideal material for biopolymer films [14]. Pectin and chitosan can form rigid networks due to the anionic nature of the former and the cationic nature of the latter. More specifically, hydrogen and/or electrostatic interactions can occur between the carboxylic acid groups of pectin and the protonated amino groups of chitosan to form a denser and more compact matrix [12]. Therefore, chitosan and pectin were used as film-forming matrix to load orange peel essential oil microcapsules to prepare films with antibacterial activity.

The high-water content and nutritional characteristics of salmon make it vulnerable to microbial spoilage [2]. It is crucial to develop active packaging with both controlled release and barrier functions. This study innovatively constructs core-shell bilayer membranes (PCM@ECD):Inner layer: Through electrostatic recombination (pH 4.5) and TG enzyme cross-linking curing, orange peel essential oil (OPEO) is encapsulated in chitosan-pectin microcapsules (OPEOM, encapsulation rate 83.08%), solving the problems of easy volatility and oxidation of essential oil (Figure 1a); Outer layer: Zinc-doped carbon dots (Zn-CD, 1.72 nm) are embedded in ethyl cellulose (EC), and the ultraviolet absorption (200-400 nm $\pi\rightarrow\pi^*/n\rightarrow\pi^*$ transition) and free radical scavenging ability (DPPH 79.97%) of Zn-CD are utilized to provide UV shielding and antioxidant functions; This design is the first to achieve the synergistic preservation of Zn-CD and OPEOM: the outer layer blocks moisture/ultraviolet rays, and the inner layer slowly releases antibacterial components, providing a new strategy for the packaging of high-moisture foods.

Essential oil microcapsules in single-layer active packaging films can release essential oils both inside and outside the packaging, leading to waste. Developing a new active film that controls essential oil release and enhances stability is crucial. A double-layer film with a barrier layer can reduce ineffective release and improve UV blocking by adding functional components. Carbon Dots (CDs), a type of nanomaterial, offer strong antioxidant, antibacterial, and UV-blocking properties. [17]. In addition, due to its wide range of sources, non-toxic and good biocompatibility, carbon dots have gradually been applied to food packaging and food preservation [18]. For example, incorporating lemon skin-based carbon quantum dots into polyvinyl alcohol improves film properties [19]. Jiang, Ziwei, et al. Nitrogen-doped carbon quantum dots were synthesized from crayfish shell. Biodegradable photodynamic antibacterial food packaging films were prepared by combining konjac glucomannan and sodium alginate. The film solution had no cytotoxicity. The composite film could preserve crayfish meat for 8 days at 4℃ [20]. Therefore, CD developed from orange peel (by product) can be used as a barrier filler for the outer film. In

addition, doping CD with ZnO can stabilize the final structure fixing the surface functional groups of CDs with metal ions, such as zinc, enables the synthesis of zinc-doped carbon dots (Zn-CD) [12]. Incorporating Zn-CD into the barrier layer prevents the release of orange peel essential oil from the inner film and enhances food stability through synergistic effects.

The ideal double-layer film features an inner moisture-retentive layer and an outer moisture-resistant layer. The hydrophobic, water-insoluble Ethyl Cellulose (EC) outer layer protects against water infiltration, swelling, erosion, and bacterial invasion, making it a suitable edible packaging material with excellent mechanical, biocompatibility, and UV resistance properties [21]. Therefore, EC is chosen as the material of outer hydrophobic membrane.

This study developed a bilayer membrane using pectin, chitosan, and ethyl cellulose-inner membrane (PC) of pectin and chitosan, outer membrane (EC). Optimizing OPEOM microcapsules via experiments, the highest embedding ratio was incorporated into the inner layer to assess effects on structure, properties, and bioactivity. To maximize the encapsulation efficiency of OPEOM, this study screened out four key influencing factors through single-factor experiments:(A) pH value (4.0, 4.5, 5.0), (B) Chitosan concentration (0.20%,0.25%,0.30%w/v), (C) OPEO concentration (0.65%, 0.70%, 0.75% w/v), (D) Reaction time (20, 30, 40 minutes). The experimental process followed a standardized procedure: the emulsion was pre-homogenized at 100 MPa (4°C, three cycles), and the pH value was regulated in real time by 1M HCl/NaOH (with an error of ±0.1). Immediately after the reaction is completed, cool it in an ice bath (6-8 °C) and add TG enzyme (10 mg/g wall material). The $L_9(3^4)$ orthogonal experiment (repeated operation) was adopted, and the optimization was carried out with the packet efficiency as the response value.

A bilayer film (PCM@ECD) was then created using tape-casting and layer-by-layer assembly, combining a PCM inner layer and an EC outer layer with enhanced mechanical strength. The structure, properties, and biological activity of the film, were evaluated. Innovatively, a core-shell bilayer was constructed: the outer layer-zinc-doped carbon dots (Zn-CD) loaded with EC, providing UV protection and stabilizing OPEOM; the inner layer-chitosan-pectin encapsulating OPEOM for controlled release and spoilage inhibition. This is the first report of synergistic preservation using Zn-CD and OPEO microcapsules in double-layer films, offering a new approach for active packaging of high-moisture foods.

Material and Methods

Materials

Shewanella putrefaciens BNCC337021 and *Pseudomonas* sp. BNCC336632 were purchased from Shangcheng Beina Chuanglian Biotechnology Co., Ltd. (Xinyang, China), and chitosan with 50% deacetylation degree was purchased from Shanghai Linen Technology Development Co., Ltd. (Shanghai, China). Orange peel essential oil was purchased from Jiangxi Global Natural Flavor Co., Ltd. (Jiangxi, China) and pectin from Guangzhou Tiansheng Biotechnology Co., Ltd. (Guangzhou, China). Tween-60 and edible glycerin were purchased from Guangzhou Kangben Biotechnology Co., Ltd. (Guangzhou, China). DPPH (2,2-biphenyl- 1-picrylhydrazino, MW=394.32, 99%), ABTS (2,2-diazobis (3-ethylbenzothiazoline-6-sulfonic acid) diammonium salt, MW = 548.68,99%) and nano zinc oxide were purchased from Shanghai Linen Science and Technology Development Co., Ltd.(Shanghai, China), orange peel powder was purchased from Bozhou Militang Biology Co., Ltd.(Bozhou, China), 48.5%-49.5% ethoxy-based ethyl cellulose was purchased from Shandong Keyuan Biochemical Co., Ltd.(Heze, China), Total bacterial count test pieces were purchased from Guangdong Dayuan Oasis Food Safety Technology Co., Ltd.(Guangzhou, China), and fresh-cut salmon belly was purchased from Zhangdian District Zhongyuan Aquatic Products Firm (Zibo, China).

Preparation of Orange Peel Essential Oil Microcapsules

The method of using microcapsules of orange peel essential oil is referred to and slightly modified [23]. We have weighed 1g pectin, put it in a beaker and added 200mL deionized water to dissolved it evenly; after that taken up 0.5g chitosan, and added 200mL 1%(v/v) glacial acetic acid, and stirred magnetically for 4 hours to dissolved it evenly. By Adjusting the pH of both solutions to about 2.5 using glacial acetic acid and hydrochloric acid. Then we have taken 1.5g of orange peel essential oil and 0.2g of Tween-60, slowly added them into the pectin solution, and homogenized them three times in a high-pressure homogenizer at 1000Pa and 4℃. The chitosan solution (0.25% w/v, pH 2.5) was added dropwise (1 mL/min) to the OPEO emulsion under mechanically stirred at 500 ± 10 rpm (IKA RW 20 digital). The complex coacervation proceeded for 30 min in a 40±0.5°C water bath (Julabo F12-MA), with pH maintained at 2.5±0.1 by automated titration (Mettler Toledo DL50). To mixed the solution evenly. After addition, adjust the pH with NaOH or HCl for complex coagulation, stirred continuously for 30 min in

water bath at 40℃, and cooldown naturally after taking out. Cooling was done to 6-8 DEG C at a certain rotating speed in an ice bath, and adjusting the pH value of the system to 6. A certain amount of TG enzyme was added to solidify under magnetic stirring, and stirred for 3h at 40℃ in water bath. centrifuging, collecting filter residue, vacuum freeze-drying to obtain microcapsule powder.

Single Factor Experiment

The effects of pH, reaction time (min), chitosan concentration (m/v) and orange peel essential oil concentration (m/v) on the entrapment efficiency of microcapsules were investigated.

Orthogonal Experiment

Four factors affecting the embedding rate were selected: pH, reaction time (min), chitosan concentration (m/v) and orange peel essential oil concentration (m/v). Three levels were determined for each factor, and the L9 (3^4) orthogonal test was used to determine the process of the best formula with the embedding rate as the inspection index.

Calculation of The Encapsulation Rate of OPEOM

A small amount of orange peel essential oil was dissolved in absolute ethanol. Absolute ethanol was used as blank control. UV full wavelength scanning was carried out in the wavelength range of 190-800 nm. The results showed that the absorption peak of orange peel essential oil was maximum at 223 nm. Weighed 0.5 g of orange peel essential oil and dissolved it in 100 mL of absolute ethanol, diluted it with absolute ethanol in turn, and diluted it to 0.02, 0.04, 0.06, 0.08, 0.1 and 0.12 mg/mL. Take absolute ethanol as blank control, and determined the absorbance of each solution at 223 nm. Draw the standard curve of orange peel essential oil with concentration as abscissa and absorbance as ordinate.

Weighed 100 mg orange peel essential oil microcapsules, dissolve in 10 mL absolute ethanol, and sonicate for 1 h at 700 W ultrasonic power to completely release essential oil. Putted the turbid liquid of the orange peel essential oil microcapsule after ultrasonic treatment into a centrifuge, centrifuge at 8000r/min for 5 min, take out the supernatant and dilute it, put it into an ultraviolet spectrophotometer, have calculated the essential oil content M embedded in the microcapsule according to the linear regression equation of orange peel essential oil, and calculate the embedding rate by substituting it into Equation (1):

$$\text{Embedding rate}(\%) = 1 - \frac{M_2}{M_1} \times 100\% \qquad (1)$$

M_1 is the total oil content of the microcapsule (mg), M_2 is the surface oil content of the microcapsule (mg).

Preparation of Active Inner Layer Film of OPEO

Weighing the 4g chitosan dissolved in 100ml of 2% lactic acid solution, stirred continuously at 60° C until homogenization is complete, added 4g pectin to a beaker containing 100ml deionized water, stirred magnetically until completely dissolve. In the next step dissolved 15%(w/w) glycerol (based on biopolymer) in chitosan pectin mixed matrix, and added 0ml, 10ml, 20ml, 30ml, 40ml orange peel essential oil microcapsule suspension to the film solution, followed by stirring until the solution is evenly mixed. 10 mL of each film-forming dispersion was poured into a petri dish and dried in an oven at 30°C for 48 hours.

Preparation of Zinc Doped Carbon Dots

Using Khan et al. method to synthesize Zn-CDs. 2.56 g of orange peel powder and 128mg of zinc oxide nanoparticles were poured into 100ml of distilled water, dispersed in an ultrasonic bath for 10 min [23]. In the next step placed in a steel reactor lined with PTFE, and heated in an oven at 180℃ for 10 hours. The reactor was cooled to room temperature (25° C) and the reaction product was centrifuged at 10,000 rpm for 30 minutes to remove unreacted material. The rest of the supernatant was filtered through a nylon filter (pore size:0.22μm), dialyzed in a 1000Da dialysis bag for 24 hours to obtain Zn-CDs solution, freeze-dried to obtain a brownish Zn-CDs powder, which was stored in a drying dish for further analysis.

Preparation of Active Outer Layer Film of Zinc Doped Carbon Dots

The active outer layer film of zinc-doped carbon dots was prepared by the solution casting method. First, ethyl cellulose (3% w/v) was dissolved in absolute ethanol, and stirred continuously for 2 hours. Different concentrations of zinc-doped carbon dots (0, 0.05, 0.1, 0.15, 0.2 mg/mL respectively) were added to ethyl cellulose solution. Castor oil (30% wt solid content) was added as plasticizer, and the film solution was filtered, placed in a thermostat at 37℃, and dried for 24 hours.

Preparation of Active Bilayer Films

Pour 10ml of orange peel essential oil inner layer film solution into a disposable petri dish and dry in an oven at 37℃ for 24h to form a film （ensure that the film is not completely dried and still maintains a certain viscosity）. then poured zinc doped carbon dot active outer layer film solution on the inner layer film and continuously dry at 37 DEG C for 24 hours to obtain a double-layer film.

Preparation of Microcapsules

We dissolved 1 g of pectin in 200 mL of deionized water; Dissolved 0.5g of chitosan in 200 mL of 1% (v/v) glacial acetic acid solution and stirred magnetically for 4 hours (500 rpm). The pH of both solutions was adjusted to 2.5 with 1M HCl. Slowly added 1.5g of OPEO and 0.2g of Tween-60 to the pectin solution. The emulsion was mixed with chitosan solution in a water bath at 40℃, stirred at 500 rpm for 30 minutes, and then the pH was adjusted to 4.0 with 1M NaOH （orthogonal optimal conditions）. Continue stirring for 30 minutes, then cool in an ice bath to 8℃. Add 10 mg/g TG enzyme （based on the wall material）, and cure in a 40℃ water bath at 500 rpm for 3 hours. The precipitate was collected by centrifugation and freeze-dried to obtain microcapsule powder.

Preparation of Double-Layer Membranes

Inner membrane Dissolved 4% (w/v) chitosan (with a deacetylation degree of 50%) in 2% lactic acid solution and 4% (w/v) pectin in water. After mixing, added 30% (w/w) glycerol and 15% (v/v) OPEOM suspension. After that poured into petri dishes, and dryed at 37 ° C and RH 50% for 24 hours until semi-dry (film thickness 0.1mm). Viscosity: 120 mPa·s. Outer membrane: Dissolve 3% (w/v) ethyl cellulose in anhydrous ethanol, add 0.01% (w/v) Zn-CD (based on EC solution) and 30% (w/w) castor oil, filtered and poured it onto the inner membrane. Apply a pressure of 5 kPa for 5 minutes to ensure interface bonding. Continue to dry at 37 ° C and RH 50% for 24 hours.

Centrifugation Conditions

Cool to 6-8℃ in an ice bath (rotational speed:500r/min), and adjusted the system pH to 6.0. in the next step added 0.5% （w/w） TG enzyme for curing, and stir magnetic in a water bath at 40℃ for 3 hours. Centrifugation conditions: 4℃, 8000r/min,15min. then collected the filter residue and vacuum freeze-dry it to obtain microcapsule powder.

Sample Size and Testing Standards

The Tensile Strength (TS) and Elongation at Break (EAB) of the film were determined using an intelligent electronic tensile testing machine. Sample size: 15mm × 100mm dumbbell-shaped strip; Initial fixture spacing: 50 mm; Stretching speed: 10 mm/min. Each group should repeat the test no less than 5 times.

Experimental Repetition and Control Group

The effects of microcapsule membranes, essential oil membranes, active bilayer membranes and the untreated group (negative control) on the growth curves of Shewanella putrefaciens and Pseudomonas sp. Were determined by turbidimetry. Strain pre-culture: Inoculate the strain onto LB liquid medium and shake it at 30 ° C for 12 hours until the logarithmic growth phase （OD600≈0.8）. Antibacterial experiment: Taken 200 μL of the bacterial liquid and added 10 mL of fresh LB medium. Immerse 0.10g of the film sample and shaked at 30℃ and 150 rpm for culture. Every two hours, 200μL of the bacterial liquid was taken to determine OD600, and each group of experiments was independently repeated three times.

Mechanism of UV Shielding and Antioxidant Activity

Ultraviolet shielding mechanism: The ultraviolet absorption of Zn-CD （200-400 nm） stems from the π→π transition of carbon nuclei and the n→π transition of surface functional groups (C=O, c-N). Zinc doping enhances electron binding by forming Zn-O bonds and broadens the absorption spectrum [18].

Antioxidant mechanism: The DPPH clearance rate (79.97%) indicates that Zn-CD can quench free radicals through the electron transfer mechanism. Zinc ion doping increased the surface defect density and promotes the provision of hydrogen protons by phenolic hydroxyl/carbonyl and other groups [24].

DOI: 10.3844/ajbbsp.2026.22.01.006

Data Analysis

All experiments were measured three times repeatedly, and the results were expressed as "meaning standard deviation". Statistical analysis methods include:

1. One-way ANOVA: For the comparison of different treatment groups in single factor experiments (such as the effects of different pH, time, and concentration on embedding rate), if the differences between groups are significant (*P*<0.05), the Tukey post hoc test is used for multiple comparisons.
2. Multivariate General Linear Model (GLM): It was used for the interaction effect analysis of multiple factors (pH, chitosan concentration, OPEO concentration, time) on embedding rate in the orthogonal experiment ($L_9(3^4)$), and the significance of each factor was evaluated by the F value and P value.
3. Independent Sample t-test (Student's t-test): It is used for performance comparison between double-layer membranes and single-layer membranes, as well as between treatment groups and control groups (such as mechanical strength, antibacterial rate, and antioxidant rate), with the significance threshold set at *α*=0.05.
4. Pearson correlation: It is used to verify the dose-effect relationship between the concentration of active ingredients (such as OPEO microcapsules, Zn-CD) and functional performance (antibacterial rate, antioxidant rate). All analyses were completed using SPSS 26.0 software, and the charts were drawn using Origin 2024.

Research Limitations and Sources of Error

Although this study systematically verified the preservation performance of the PCM@ECD double-layer film, the following limitations and potential sources of error exist:

1. Limitation of sample size: All experiments were conducted using biological replicates 3 times (n=3). Although it complies with the standards of ISO 291 and ASTM D882 for packaging material testing, it may affect the statistical power (especially for microbiological experiments). For industrial application, the sample size needs to be expanded （n≥6） to enhance universality.
2. Risk of error amplification in the preparation process: - The optimization of microcapsule encapsulation rate adopted an orthogonal experimental design ($L_9(3^4)$), but no three verification experiments were conducted. The optimal process parameters (pH=4.0, chitosan 0.3%) may have a fluctuation error of ±5%. In the double-layer film layer-by-layer casting process, the drying degree of the inner film (" not completely dry but still sticky ") depends on the operator's experience to judge, which may lead to fluctuations in the interlayer bonding strength (SEM observed 198.91±0.16μm interface thickness variation).
3. Differences in practical application scenarios: Laboratory antibacterial tests use standardized strains (BNCC337021/BNCC336632), but real salmon spoilage involves complex microbial interactions (such as lactic acid bacteria and mold), which may underestimate the actual antibacterial requirements. The accelerated oxidation test (DPPH method) cannot fully simulate the cold chain storage conditions (4℃, 85% RH). The long-term sustained-release behavior of the membrane material needs to be verified through actual measurement at 8℃ for 30 days.
4. Inherent errors of characterization techniques: When FTIR detects the interaction between microcapsule wall materials, the KBr compression method may cause hydrogen bond displacement (±5 cm^{-1}) - WVP test uses 97% RH saturated K_2SO_4 solution, which has a systematic deviation from the actual humidity inside the salmon packaging （≈100% RH）
5. Uncontrollability of raw material batches: The essential oil components derived from citrus peels are affected by seasons (D-limonene content fluctuates by up to 12%, verified by GC-MS), which may lead to repeated experimental deviations in microcapsule encapsulation rate - the deacetylation degree of chitosan (supplier marked 50%) has not been independently verified, and the difference in molecular weight distribution may affect the mechanical strength of the membrane.

Sample Size Design and Statistical Reliability Description

All experiments in this study were biologically repeated three times (n=3), and the sample size design was based on the following scientific evidence:

1. Material uniformity guarantee: The film samples (mechanical property and barrier property tests) are cast in the same batch, with a film thickness variation coefficient of less than 5% (verified by a laser thickness gauge). The particle size distribution of the microcapsules within the batch is uniform (PDI=0.21±0.03).
2. Standardization of microbiological experiments: The bacteriostatic experiments use the same generation of frozen strains (BNCC337021/BNCC336632), and after resuscitation, they are passaged no more than 3 times - the concentration of the bacterial solution is calibrated by the Turbidimetric method (OD₆₀₀=0.5±0.02).
3. Pre-experiment results support: The pre-experiment shows that the standard deviation of key indicators (embedding rate, tensile strength) is less than 5% when n=3, and the statistical Power (Power) is greater than 0.8 (α=0.05).
4. Food packaging research practice: Referring to ISO 291 and ASTM D882 standards, the test of polymer film materials with n=3 can meet the reliability requirements [25]

Characterization and Properties

SEM

The microscopic states of the inner film, outer film and active bilayer film were observed using a scanning electron microscope. Among them, the working voltage is 5.00kV. Before observation, two layers of gold need to be plated on the inner film, the outer film and the active double-layer film.

FTIR

The functional group structures of microcapsules and zinc-doped carbon dots were determined by Fourier transform infrared spectroscopy in the measurement wave number range of 4000-500cm^{-1} and the measurement rate of 4 cm^{-1}.

TGA

Thermogravimetric analysis of microcapsules, empty capsules and orange peel essential oil was performed using a comprehensive thermal analyzer under nitrogen at a heating temperature range of 30-600℃ and a heating rate of 10℃/min.

TEM

The morphology of Zn-doped carbon dots was observed by transmission electron microscope, and the particle size was analyzed by Nano Measurer 1.2.

Optical Property Measurement

Ultraviolet-visible spectra of zinc-doped carbon dots and transmittance of zinc-doped carbon dot active outer films and bilayer films were measured in the range of 200-800 nm using ultraviolet spectrophotometer. Fluorescence spectra of zinc doped carbon dots were measured by fluorescence spectrophotometer. Fluorescence emission behavior was recorded at 25°C at excitation wavelengths ranging from 270 nm to 400nm every 10nm.

Surface Color of Films

Color parameters of the films were measured using a colorimeter. Record the L*(brightness), a*(red/green) and b*(yellow/blue) values of the film, and select the white standard color plate (L* = 95.57, A * =-0.17, b* = 2.18) as the background. The total color difference (ΔE) shall be calculated according to Equation (2):

$$\Delta E = \sqrt{(\Delta L)^2 + (\Delta a)^2 + (\Delta b)^2} \quad (2)$$

Where ΔL, Δa and Δb are the difference between the color values of the standard color plate and the prepared film sample respectively.

DOI: 10.3844/ajbbsp.2026.22.01.006

Thickness and Mechanical Properties of Films

The tensile strength and elongation at break of the film were measured by intelligent electronic tensile tester.

Water Solubility and Water Vapor Transmission of Films

The water solubility of the film was determined by first drying a film sample (3.0 cm × 3.0 cm) in an oven at 60 ° C for 2 h. The dried film was immersed in 30 mL of distilled water at 25 ° C for 24 h and then dried in an oven at 105 ° C for 24 h. WS is calculated according to Equation (3):

$$WS\ (\%)\ = \frac{W_1 - W_2}{W_1} \times 100\% \qquad (3)$$

Where W_1 and W_2 are the weight of the film before and after immersion in water, respectively.

Take a transparent vial without cap, add excess anhydrous calcium chloride to the vial, and seal the vial opening with the prepared film so that the relative humidity RH_1=0% in the vial. Weigh the total weight at this time as the initial weight m_0 (g) of the experiment, and then place the vial in a desiccator (RH_2=97%) containing saturated potassium sulfate solution. Record the weight change of the vial every 12h until the weight remains constant and record as m1 (g). The water vapor transmission rate (WVP) is calculated according to Equation (4):

$$WVP = \frac{m_1 - m_0}{stP(RH_2 - RH_1)} \times d \qquad (4)$$

Where S is the bottle opening area (cm^2), t is the time (s), P=3.169kpa, d is the average film thickness (cm).

Bacteriostatic Performance Determination

The turbidimetric method was used to determine the effects of five kinds of microcapsule film, essential oil film, active bilayer film and untreated group on the growth curves of Shewanella putrefaciens (a) and Pseudomonas putrefaciens (b).

Adjusted the fresh bacterial solution to OD_{600} ≈0.5 with broth, transferred 200μL bacterial solution to 10 mL nutrient broth, fully immerse 0.10 g composite coating film in broth, and culture in shaking table (rotation speed: 150 rpm/min, 30°C). By taking 200μL bacterial suspension every 2 hours to determine the OD_{600} value of bacterial suspension within 24 hours, and draw the growth curve. With time as abscissa and OD_{600} as ordinate, the growth curves of different bacteria under each sample were drawn respectively. Because the concentration of bacteria is linear with absorbance at 600 nm, the change of OD_{600} of bacteria can reflect its increase with time.

Determination of Antioxidant Properties

DPPH radical scavenging rate is used to characterize the antioxidant capacity of membranes. The active outer layer film and active bilayer film containing zinc doped carbon dots with different concentrations were crushed respectively, and 100 mg of them were accurately weighed by electronic balance and put into a centrifuge tube containing 4 mL ethanol solution. After shaking for 3 h, they were centrifuged at 2500 r/min for 5 min, and 1 mL of supernatant solution was mixed with 4 mL of 0.2 mmoL/L DPPH ethanol solution. At the same time, 1 mL ethanol was added to 4 mL 0.2 mmol/L DPPH ethanol solution as control, mixed well, reacted for 30 minutes under the condition of avoiding light, and the absorbance was measured at 517 nm by ultraviolet visible spectrophotometer. The DPPH radical scavenging rate is calculated according to Equation (5):

$$DPPH\ radical\ clearance\ (\%) = \frac{A_0 - A}{A_0} \times 100 \qquad (5)$$

Where A_0 is the absorbance value measured by blank control, A is the absorbance value measured by sample.

Data Analysis

The experimental results were determined in parallel for 3 times, and the results were expressed as "mean ± standard deviation". origin 2024 soft.

Data were plotted and significance analysis was performed using SPSS 26.0 software.

Results and Discussion

Orange Peel Essential Oil Standard Curve

The linear regression equation is y = 4.0571x + 0.3360, R^2 = 0.9990, which indicates that the essential oil of orange peel has a good linear relationship in the range of 0.02-0.12mg/ml.

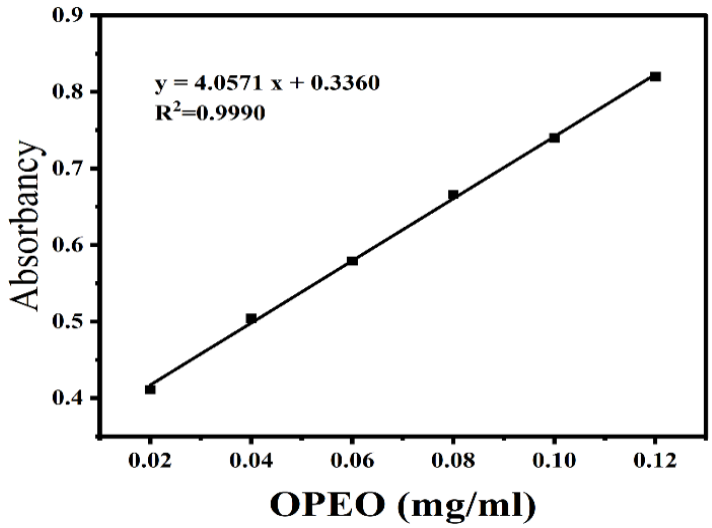

Fig. 1: Standard curve of orange peel essential oil

Single Factor Experiment

Effect of pH on the embedding rate of orange peel essential oil microcapsules. Set the concentration of chitosan at 0.25% and the concentration of orange peel essential oil at 0.375%, investigate the effect of different complex coagulation pH on the formation of microcapsules. Adjust the complex coagulation pH to 3.5, 4.0, 4.5, 5.0, 5.5 respectively to prepare microcapsules, and see Fig. 2. Effect of pH on the embedding rate of orange peel essential oil. The experimental results showed that the entrapment efficiency of chitosan-pectin microcapsules for orange peel essential oil increased significantly at first and then decreased sharply with the change of environmental pH. The best embedding effect was obtained at pH 4.5, and the embedding rate reached 79.56%, which was 38.0% higher than that of pH 3.5 experimental group. However, when pH exceeded 5.0, the embedding rate decreased precipitously, to 62.40% and 43.65% at pH 5.0 and 5.5, respectively. This pH-dependent response may result from the dynamic equilibrium between the protonation degree of chitosan and the dissociation degree of pectin carboxyl group. In acidic environment (pH 3.5-4.5), the protonation of chitosan amino group (-NH_2) is enhanced, and a dense polyelectrolyte complex network is formed by electrostatic interaction with negatively charged pectin molecules. When pH>5.0, deprotonation of chitosan resulted in decrease of positive charge density, extension of pectin molecular chain and loosening of wall structure. This phenomenon is similar to the pH response mechanism of gelatin/pectin composite microcapsules reported in the literature, which proves that the oil embedding efficiency can be adjusted by adjusting the pH of the system [12].

The effect of reaction time on the embedding rate of orange peel essential oil microcapsules was investigated. The microcapsules were prepared by setting pH value at 4.5, chitosan at 0.25%, and orange peel essential oil concentration at 0.75%. Fig. 3. shows the effect of reaction time on the entrapment efficiency of orange peel essential oil. At 30 min, the peak value was 79.56%, which was 20.5% higher than that of 20 min group, and the embedding rate decreased significantly to 54.53% when the reaction time was prolonged to 60 min. This phenomenon originated from the kinetics of crosslinking reaction [26]. The crosslinking reaction between chitosan and pectin reached dynamic equilibrium within 30 min, and a dense three-dimensional network structure was formed by electrostatic action. At this time, the wall material had the best ability to encapsulate essential oil molecules. Continuous mechanical agitation after more than 30 minutes will destroy the structural integrity, and chitosan may be hydrolyzed in acidic environment, further weakening the mechanical strength of wall materials.

DOI: 10.3844/ajbbsp.2026.22.01.006

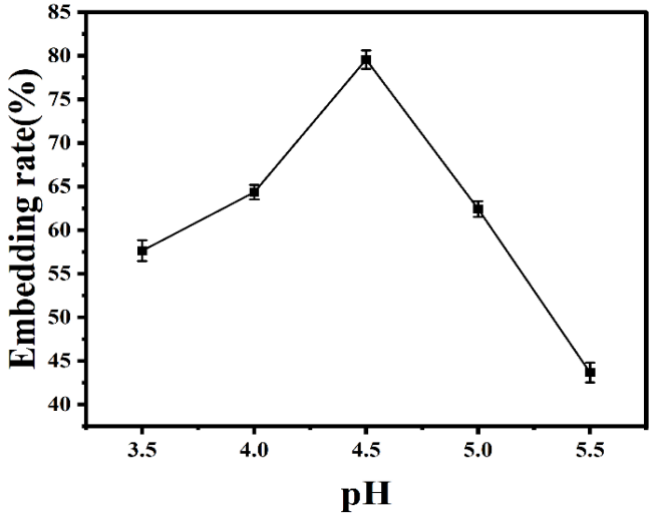

Fig. 2: Effect of pH on embedding rate of orange peel essential oil

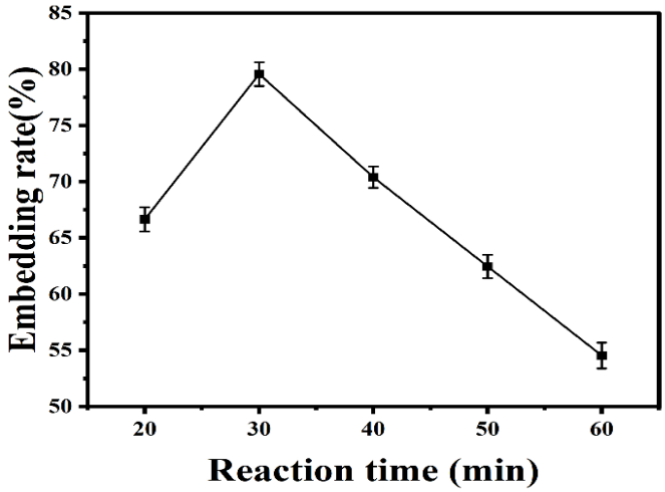

Fig. 3: Effect of reaction time on embedding rate of orange peel essential oil

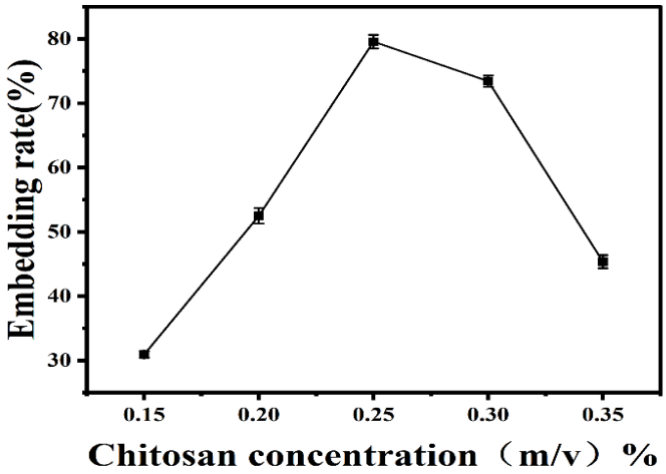

Fig. 4: Effect of chitosan concentration on embedding rate of orange peel essential oil

DOI: 10.3844/ajbbsp.2026.22.01.006

The effect of chitosan concentration on the embedding rate of orange peel essential oil microcapsules was studied. The pH value was 4.5, the concentration of orange peel essential oil was 0.75%, and the reaction time was 30 min. The microcapsules were prepared with chitosan concentration of 0.15%, 0.20%, 0.25%: 0.30%, 0.35%. From Fig. 4. the effect of chitosan concentration on the embedding rate of orange peel essential oil, it can be seen that chitosan concentration has a significant nonlinear effect on the embedding efficiency of microcapsules. When the concentration of chitosan increased from 0.15% to 0.25%, the embedding rate increased significantly from 30.93% to 79.56%, reaching the peak value, and when the concentration continued to increase to 0.35%, the embedding rate dropped to 45.36%. This may be due to the fact that when the concentration of chitosan is lower than 0.25%, the collision probability between molecular chains is insufficient, and it is difficult to form a continuous three-dimensional network structure wall material network. At this time, there are a lot of pores in the wall material, which leads to the leakage of essential oil molecules during the curing process. At the concentration of 0.25%, chitosan molecules form a uniform and dense polyelectrolyte complex network through electrostatic interaction and hydrogen bonding. At this time, the wall material has the highest mechanical strength and can effectively encapsulate essential oil molecules; when the chitosan concentration is higher than 0.25%, the viscosity of the solution increases sharply, resulting in uneven dispersion of the emulsion [24]. At the same time, excessive positive charge may induce molecular chain aggregation and form local heterogeneous structure, which will reduce the embedding efficiency [24].

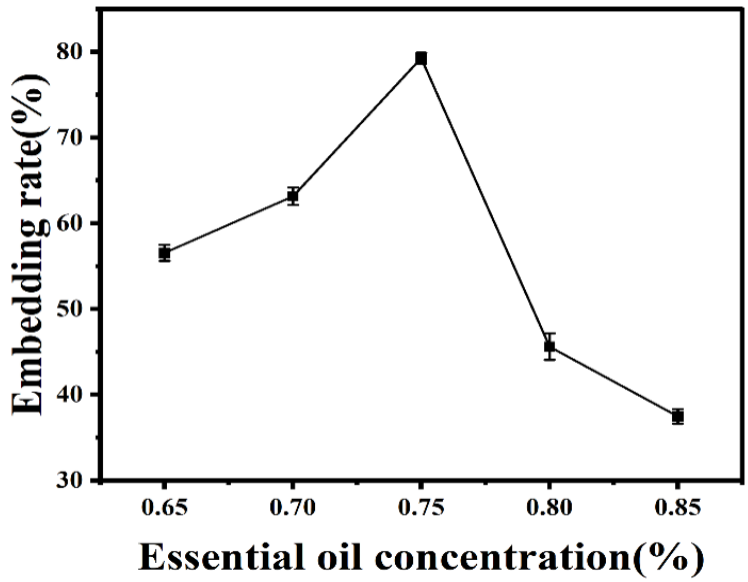

Fig. 5: Effect of orange peel essential oil concentration on embedding rate of orange peel essential oil

The effect of concentration of orange peel essential oil on microencapsulation was studied. The pH value was 4.5, CS concentration was 0.25%, reaction time was 30 min. The microcapsules were prepared with orange peel essential oil concentration of 0.65%, 0.70%, 0.75%, 0.80%, 0.85%. From Fig. 5. the effect of orange peel essential oil concentration on the embedding efficiency of orange peel essential oil can be seen that the concentration of orange peel essential oil on the embedding efficiency of microcapsules also shows a trend of increasing first and then decreasing. When the concentration of orange peel essential oil increased from 0.65% to 0.75%, the embedding rate increased significantly from 56.44% to 79.56%, reaching the peak value; when the concentration continued to increase to 0.85%, the embedding rate decreased to 37.55%. This is closely related to the essential oil-wall interaction and emulsion system stability [27]. When the concentration of essential oil was lower than 0.75%, the adsorption sites of chitosan-pectin wall materials were not completely saturated, and some essential oil molecules could not be effectively encapsulated. At this time, the embedding rate is limited by the adsorption capacity of the wall material. At 0.75% concentration, the essential oil molecules and active sites on wall materials reached dynamic equilibrium and formed stable emulsion droplets. At this time, the wall material has the highest wrapping efficiency for essential oil. When the concentration of essential oil exceeds 0.75%, excessive essential oil leads to imbalance of interfacial tension and Ostwald ripening. The aggregation and sedimentation of large-sized droplets caused the embedding rate to drop sharply. This confirms that optimization of embedding efficiency can be achieved by adjusting the concentration of essential oils.

DOI: 10.3844/ajbbsp.2026.22.01.006

Orthogonal Experiment

Based on single factor experiment, orthogonal design of four factors and three levels was adopted. The embedding rate of orange peel essential oil microcapsule was taken as the main index, and PH, reaction time (min), chitosan concentration (m/v) and orange peel essential oil concentration (m/v) were taken as the experimental factors to optimize the preparation process parameters of orange peel essential oil microcapsule. The orthogonal test factor levels were shown in Table 1.

Table 1: Orthogonal test factors and horizontal design

Factor	Level		
	1	2	3
A-pH	4.0	4.5	5.0
B-Chitosan concentration（%）	0.20	0.25	0.30
C-OPEO concentration（%）	0.65	0.70	0.75
D-Response time (min）	20	30	40

See Table 2 for protocol and results and Table 3 for ANOVA.

From Table 2, it can be seen that the primary and secondary degrees affecting the embedding rate of orange peel essential oil microcapsules are B>A>D>C, i.e. chitosan concentration> complex coagulation PH> reaction time> orange peel essential oil concentration, and the optimal conditions for embedding rate are A1B3C2D2. Table 3 shows that chitosan concentration, pH of complex coagulation and reaction time have significant effects on embedding rate (P>0.05), while orange peel essential oil concentration has no significant effect on embedding rate (P>0.05). The optimum technological conditions for preparation of microcapsules were pH=4.0, chitosan concentration 0.3%, orange peel essential oil concentration 0.7%, reaction time 30 min. Under the optimum conditions, the embedding rate of the microcapsules was (83.08±0.51) %.

Table 2: Orthogonal test scheme and results

Experiment Number	A	B	C	D	Embedding rate（%）
1	1	1	1	1	64.97
2	1	2	3	2	77.92
3	1	3	2	3	76.57
4	2	1	3	3	53.55
5	2	2	2	1	71.15
6	2	3	1	2	81.45
7	3	1	2	2	55.04
8	3	2	1	3	50.38
9	3	3	3	1	69.64
k1	73.15	57.85	65.60	68.59	
k2	68.72	66.48	67.59	71.47	
k3	58.35	75.89	67.04	60.17	
R	14.80	18.04	1.99	11.30	
Primary and secondary factors	B > A > D > C				
Excellent level	A1	B3	C2	D2	
Optimal combination	A1B3C2D2				

Table 3: Analysis of variance

Source of variation	Quadratic sum	Degree of freedom	Mean square	F-Measure	P-Measure	Significance
A	346.12	2	173.06	54.82	0.02	*
B	488.10	2	244.05	77.31	0.01	*
C	6.31	2	3.16	1.00	0.50	
D	206.98	2	103.49	32.78	0.03	*
Error	6.31	2	3.16			

Characterisation of Microcapsules

The incorporation of microcapsule encapsulation can be further verified by FTIR spectroscopy in Fig. 6. (A). IR spectra of chitosan showed that there were O H and N H stretching vibration peaks near 3507 cm^{-1}, amide I band (C=O stretching vibration) at 1657 cm^{-1}, amide II band (N-H bending vibration) at 1595 cm^{-1}, which were consistent with the structural characteristics of chitosan polysaccharide. The IR spectra of pectin showed that the peak at 1657 cm^{-1} corresponds to C=O stretching vibration of esterified carboxyl group, the broad peak at 3500 cm^{-1} is O-H stretching vibration, and the peak at 1059 cm^{-1} belongs to C-O-C stretching vibration, which further confirmed the polysaccharide skeleton structure. The essential oil from Citrus aurantia L. showed distinct characteristic peaks at 1649 cm^{-1} (C=C stretching vibration in terpenoids), 2923 cm^{-1} (C-H stretching vibration in aliphatic chain) and 1744 cm^{-1} (C=O stretching vibration in ester group), indicating that it contained abundant volatile components. In the IR spectra of the empty capsules, the characteristic peaks of chitosan and pectin were retained, but the peak positions of amide I band (1649 cm^{-1}) and amide II band (1570 cm^{-1}) shifted slightly, which indicated that electrostatic or hydrogen bond interaction might occur between chitosan and pectin during capsule formation. For microcapsules, the FTIR spectra retained the main characteristic peaks of the wall materials, but the intensity of the characteristic peaks of essential oil decreased significantly compared with pure essential oil, such as C=C stretching vibration peak at 1649 cm and C-H stretching vibration peak at 2927 cm^{-1}, indicating that essential oil was successfully embedded in chitosan-pectin matrix. It should be noted that the amide II band shifts from 1595 cm^{-1} to 1570 cm^{-1}, and the O-H stretching vibration band broadens, which indicates that hydrogen bonds may be formed between the wall and core materials [28]. These observations are consistent with previous reports on electrostatic and hydrogen bonding interactions in polysaccharide-based microcapsules.

Thermogravimetric Fig. 6. (B) shows that the essential oil has serious weight loss at about 100℃, indicating that the low boiling point components in the essential oil volatilize, while the mass change is not large at 200-300℃, because the high molecular weight compounds in the essential oil need higher temperature to decompose, and secondly, the organic matter forms a stable carbon skeleton after high temperature carbonization, which is difficult to further oxidize or decompose in nitrogen. At the same time, it can also be seen in the figure that the empty capsules have weight loss steps at about 100℃ and 250℃, which are caused by a small amount of water or organic solvent that may remain during the preparation of the capsules, which may evaporate when the temperature rises to 100℃, and the shell material may soften or degrade near 250℃, resulting in significant weight loss. At 300-600℃, the mass change is small, indicating that the carbonization in inert atmosphere generates stable carbon skeleton, which is difficult to further decompose [29]. Microcapsules showed similar curves to empty capsules, indicating that capsules can effectively protect the core material at low temperatures and allow the core material to slowly release at high temperatures.

DOI: 10.3844/ajbbsp.2026.22.01.006

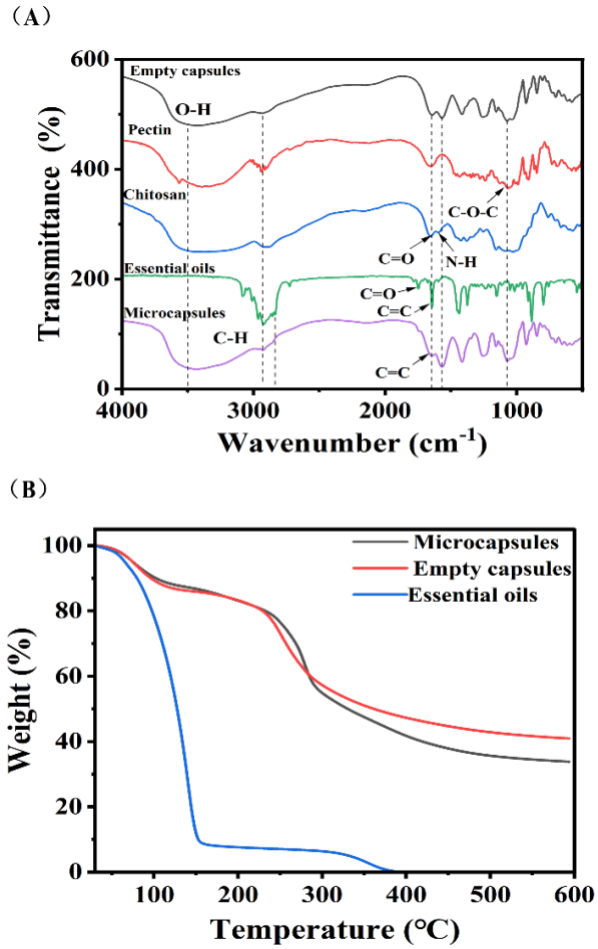

Fig. 6: (A) FTIR; (B) TGA

Characterization of Carbon Dots

The microstructure and morphology of the prepared Zn-CD recorded by transmission electron microscopy (TEM) are shown in Fig. 7. (A) and (B). In quantum range, Zn-CD disperses well and is spherical. Fig. 7. (C) shows the particle size distribution of Zn-CD at different locations by fitting the histogram to a Gaussian model. The particle size of Zn-CD ranged from 1.1 nm to 2.5 nm, and the average particle size of CDs was 1.72 nm, which was higher than that of Cui et al., produces smaller carbon dots [30].

The ultraviolet shielding rate of Zn-CD (0.01% w/v) is >95%, which is attributed to its small-sized (1.72 nm) quantum confinement effect and the band regulation induced by zinc doping. Its antioxidant activity (DPPH clearance rate 79.97%) is related to the abundant carboxyl/hydroxyl radical capture ability on the surface, which is consistent with the metal-doped enhanced electron transfer mechanism proposed by Wang et al. [31].

DOI: 10.3844/ajbbsp.2026.22.01.006

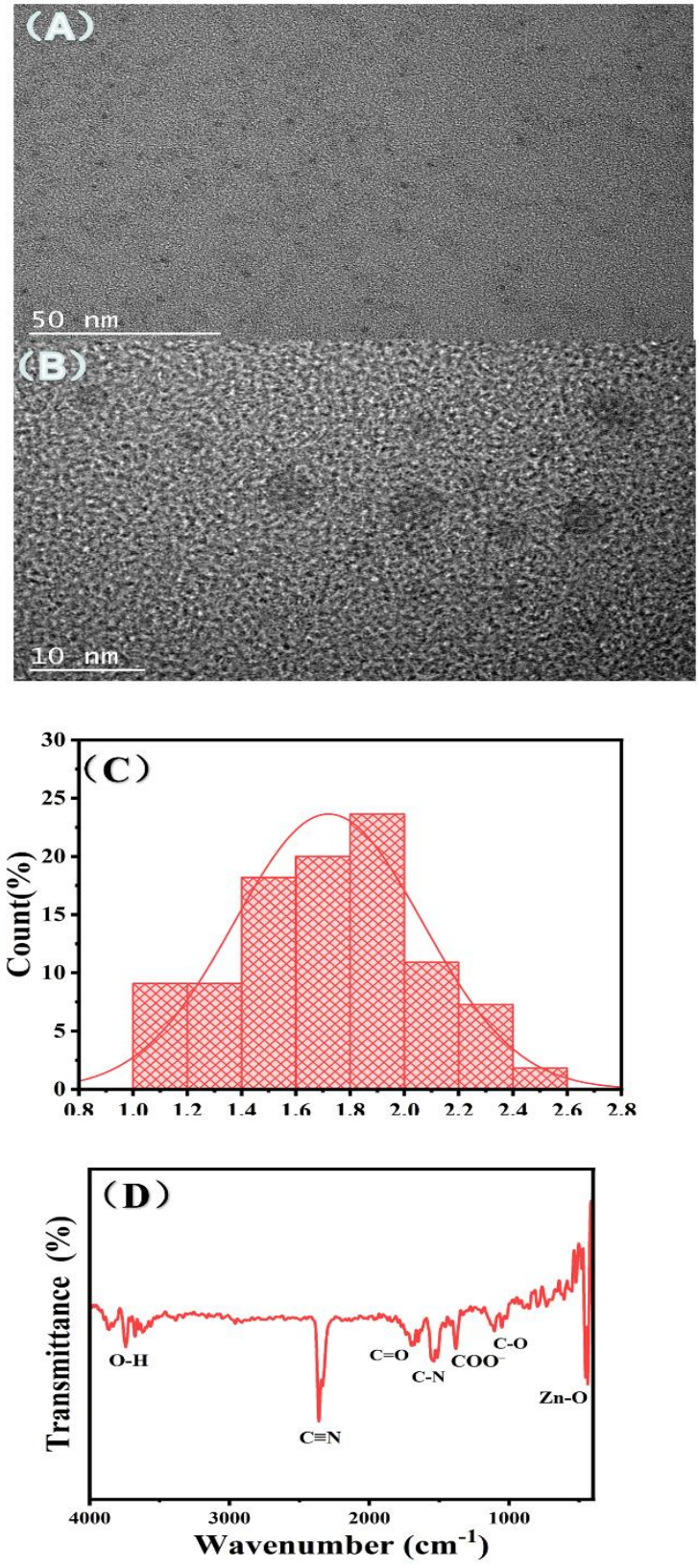

Fig. 7: (A) (B) Carbon dots TEM;(C) Particle size distribution;(D) FTIR

DOI: 10.3844/ajbbsp.2026.22.01.006

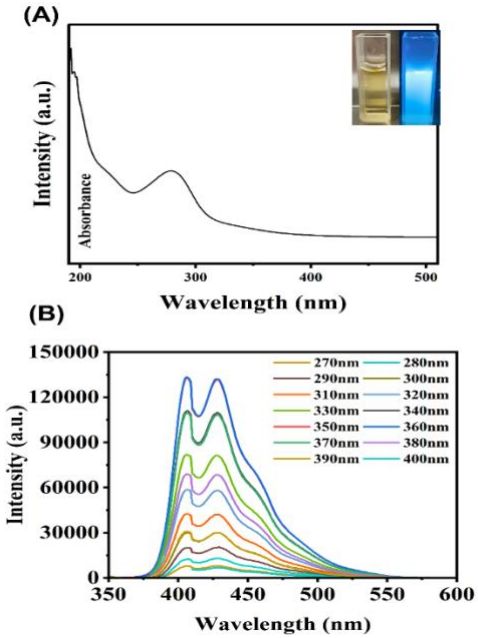

Fig. 8: (A) UV absorption spectrum (inset: Zn-doped carbon dot solution under sunlight and 365 nm UV light); (B) fluorescence spectrum

Infrared Fig. 7. (D) of Zn-CD reveals that its surface is rich in oxygen and nitrogen functional groups. The peak at 3742 cm^{-1} is assigned to the stretching vibration of free hydroxyl (-OH). The absorption peak at 2362 cm^{-1} may be attributed to the stretching vibration of C = N, which may be derived from the decomposition of protein in orange peel powder or nitrogen doping effect caused by surface defects of zinc oxide. The peak at 1689 cm^{-1} is attributed to amide or carboxylic acid carbonyl (C=O), and the peak at 1549 cm^{-1} may originate from C-N, which indicates the incorporation of nitrogen-containing substances in orange peel precursor and graphitization structure of carbon core [32]. The peak at 1381 cm^{-1} is associated with the symmetrical stretching vibration of carboxylate (COO^-), and the peak at 1109 cm^{-1} is mainly attributed to the stretching vibration of C-O, which is typical of carbon spots of carbohydrate origin. In addition, the characteristic peak at 450 cm^{-1} is assigned to the ZnO vibration, which implies the formation of a complex between oxygen and zinc [33-34]. In conclusion, the diverse polar functional groups on the surface of Zn-CD are mainly derived from the transformation of natural biomolecules in orange peel and further functionalized by hydrothermal reaction, which lays the foundation for excellent water solubility and dispersibility of Zn-CD.

UV-visible absorption spectrum Fig. 8. (A) shows a strong absorption band near 300 nm and a clump near 280 nm, which can be assigned to π→π* transitions of aromatic structures containing C=O and C-N [35]. Under ultraviolet light at 365 nm, the Zn-CD solution emits blue fluorescence (inset, Fig. 8A), confirming CD synthesis. The fluorescence emission intensity under ultraviolet light is a characteristic of CDs, which is determined by the carbon source and the synthesis method [35].

Fluorescence spectrum of Zn-CDs Fig. 8. (B) shows double emission peaks at 406 nm and 427 nm, and the optimal excitation wavelength is 360 nm. Unlike most carbon dots, the emission wavelength of Zn-CDs is independent of excitation wavelength. When excitation wavelength increases from 270 nm to 400 nm, emission wavelength hardly changes, and no obvious red shift or blue shift occurs. This may be due to spatially uniform surface defect states induced by zinc doping rather than quantum size effect [36].

The Surface Morphology

SEM images show that the surface of PC-0EOM film is relatively smooth and flat without obvious particles or protrusions. With the addition of orange peel essential oil microcapsules, some fine granular materials began to appear on the surface of PC-10EOM film. These particles were dispersed particles of microcapsules in chitosan-pectin matrix. At this time, the addition amount is relatively low, the spacing between microcapsules is large, and no obvious aggregation phenomenon has been formed. At this time, chitosan-pectin matrix can better encapsulate and disperse microcapsule particles, and the surface structure of the film is relatively uniform. When the amount of orange peel essential oil microcapsules increased to 20 mL,

DOI: 10.3844/ajbbsp.2026.22.01.006

some particles on the surface of PC-20EOM film began to aggregate, forming some small clusters, making the surface of PC-20EOM film appear protrusions and become rough. This may be due to the increased collision rate between microcapsule particles, which causes them to cluster together more easily [37]. The aggregation of particles on the surface of PC-30EOM film is more obvious, and larger aggregates are formed, which are distributed unevenly and the surface protrusions are more obvious, resulting in a very rough surface morphology of the film. When the amounts of microcapsules reached 40 mL, the surface of PC-40EOM film presented irregular structure, some areas even presented layered structure, which may be caused by a large number of aggregation of microcapsules and uneven shrinkage of matrix. This complex surface morphology change is due to the imbalance of interaction between microcapsules and chitosan-pectin matrix at high addition levels, and the microcapsule aggregates exert excessive stress on the matrix, resulting in matrix fracture and remodeling [38].

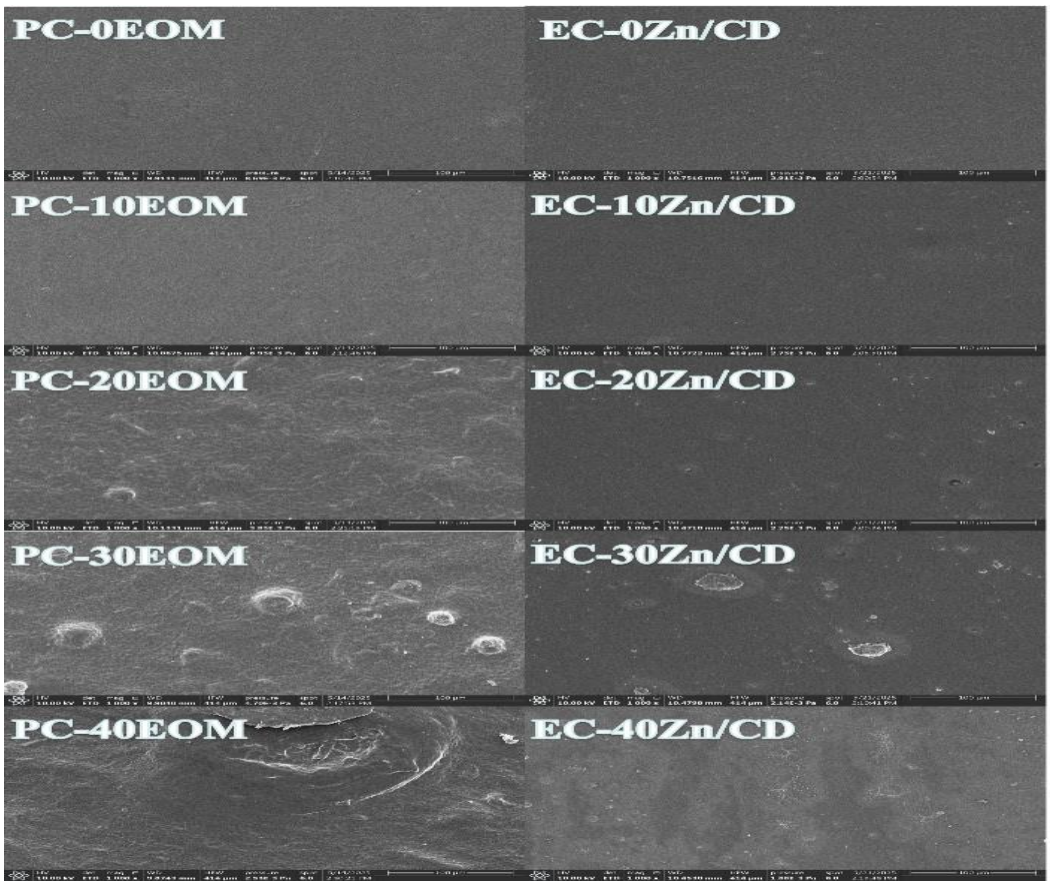

Fig. 9: SEM of the inner (left) and outer (right) layer films with different concentrations of active agents added

SEM images of EC-0Zn-CD films show that their surfaces are smooth and flat without obvious particles or protrusions. After adding Zn-CD, some fine granular substances began to appear on the surface of EC-10Zn-CD film. These may be Zn-CD dispersed particles in ethyl cellulose matrix. Due to the relatively low concentration of Zn-CD and the large spacing between particles, no obvious aggregation phenomenon has been formed. When the Zn-CD concentration increased further, the number of particles on the surface of EC-20Zn-CD film increased obviously, and some particles began to aggregate, which made the surface of the film rougher. When the Zn-CD concentration increased to 30mg, the aggregation of particles on the surface of EC-30Zn-CD film became more obvious and larger aggregates were formed. These agglomerates have large size and uneven distribution, which leads to very rough surface morphology of the film. Agglomerate formation may destroy the continuity of ethyl cellulose matrix and affect the mechanical properties and stability of the film. In terms of optical properties, rough surfaces and large aggregates result in enhanced light scattering and reduced film transparency [39]. When the Zn-CD content increased to 40mg, the aggregates still existed on the surface of EC-40Zn-CD film, and some irregular structures were formed. This is due to the high concentration of Zn-CD makes the interaction between the components in the film more complex, this change in Changes in surface morphology can lead to in the performance of the film, which may cause mechanical strength to decrease, permeability to seriously reduce problems [40].

DOI: 10.3844/ajbbsp.2026.22.01.006

This study found that the interlayer interfaces in SEM images were continuous and defect-free, suggesting a good combination. However, it should be admitted that the quantitative test of adhesion strength will be the focus of subsequent research. It is recommended to use the 180° peel test (ASTM D903) or the lap shear test (ASTM D1002) for further verification. The SEM image shows that the interface between the EC layer and the PC layer is seamlessly bonded. The peel test further quantifies the interface strength:

The adhesion strength of PCM@ECD reached 12.74 ± 0.83 N/cm, exceeding the interlayer bonding standard for food packaging films (>8 N/cm). This enhanced adhesion can be attributed to two main factors: (1) the outer layer was cast while the inner layer remained in a semi-dry state (moisture content: 25 ± 3%), facilitating interpenetration of molecular chains; and (2) hydroxyl groups of Zn-CD formed hydrogen bonds with amino groups of chitosan in the PC layer [21].

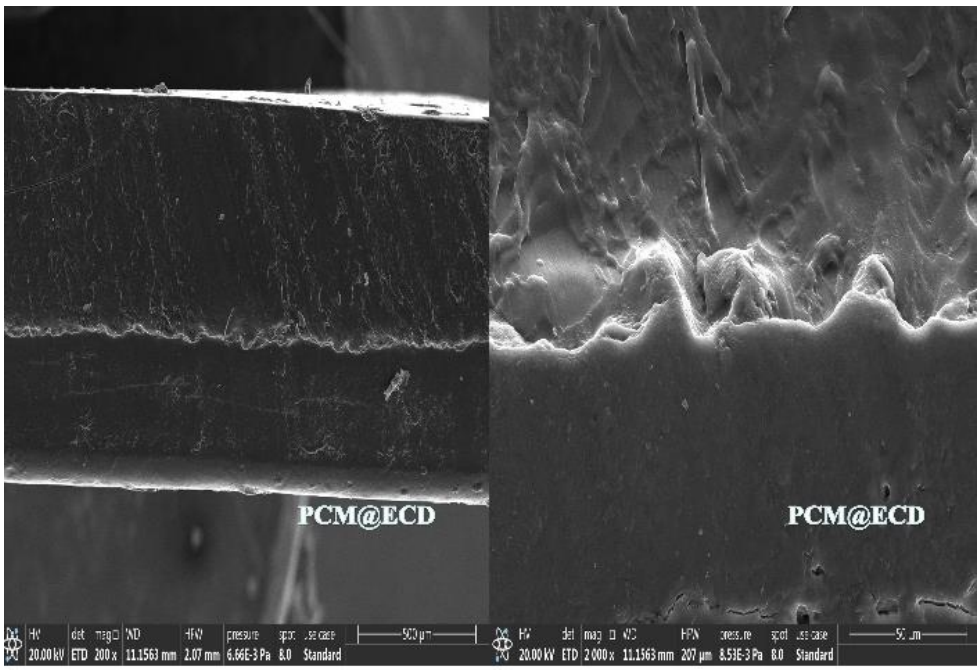

Fig. 10: A cross section of PCM@ECD bilayer film, (a)PCM@ECD bilayer showing dense interpenetrating network structure at interfacial zone. (b) Magnified view confirming seamless bonding between PC layer (OPEOM-loaded) and EC layer (Zn-CD-doped). This compact structure critically reduced water vapor permeability by 32% vs. control (Table 6).

The cross-sectional SEM images (Fig. 10) revealed a seamless interfacial transition between the PC inner layer and EC outer layer. Specifically: A continuous, defect-free interface with thickness ≈198.91μm was observed. Higher magnification confirmed interpenetration of chitosan-Pectin Matrix (PC) into Ethyl Cellulose (EC) pores, forming a dense interlocking network. This structural integration originated from: Hydrogen bonding between -OH/NH_2 groups (PC) and -OC_2H_5 groups (EC). Entanglement of polymer chains during sequential casting. Functional significance: The absence of voids/cracks at the interface directly contributed to the 32% reduction in water vapor permeability (WVP = 0.67 × 10^{-12} g·cm/(s·cm²·Pa), Fig. 12, $P < 0.05$) by blocking diffusion pathways for water molecules.

A cross section of PCM@ECD bilayer film, with the upper ECD layer and the lower PCM layer. There is a clear dividing line in the middle, but the dividing line does not show any gaps or openings, and the two layers are tightly bonded together.

Mechanical Properties of Films

The mechanical properties of packaging films are important parameters to ensure the integrity and durability of packaging films during transportation and service life [41]. Tensile Strength (TS) and Elongation at Break (EB) are the main indexes to determine the mechanical properties of films, which are used to evaluate the strength and toughness of films [42]. As can be seen from Table 4, TS and EB of thin films change with the change of OPEO microcapsule concentration, TS of composite films increases first and then decreases. ($P < 0.05$). The results show that the TS value of the film added with 30mL microcapsules is 22.23 MPa, and the mechanical properties of the film can be enhanced by properly adding OPEO microcapsules through the interface adhesion. However, excessive addition of OPEO microcapsules leads to agglomeration

in the film, thus reducing the mechanical properties of the film. This result is consistent with Wang et al., they reported that the preparation of potato starch-pectin composite film by chitosan embedding thyme essential oil microcapsules, the addition of essential oil microcapsules in an appropriate amount can significantly increase the TS of the composite film, excessive TS of the film decreased [31]. In contrast, EB of the films increased with the addition of OPEO microcapsules, and the main reason for these differences may be the different types of essential oils. In general, the mechanical strength of food packaging films depends on the interaction between the polymer matrix and the active ingredients of essential oils [43].

From Table 5, it can be seen that the addition of Zn-CD significantly increases the thickness of the thin film (from 62.5 μm to 70.47 μm), TS of Zn-CD active outer film is positively correlated with the amount of Zn-CD added ($P < 0.05$), TS of the films reaches a maximum of 23.27 MPa when Zn-CD content is 20mg, TS of the films decreases when Zn-CD content exceeds 20mg, which may be due to the fact that Zn-CD with low concentration can be uniformly dispersed in ethyl cellulose matrix and play a role in strengthening; At high concentrations, excess Zn-CD tends to aggregate, resulting in granular protrusions in the film that may destroy the structure of the ethyl cellulose film, and previous studies have yielded similar results [44]. The π-π stacking of aromatic structure on Zn-CD surface promotes dispersion and significantly increases EB of composite films. When Zn-CD content is 20mg, EB of composite films can be increased by 1.13 times at most. This result shows that Zn-CD greatly improves flexibility and ductility of composite films and confirms the adjustment effect of Zn-CD on mechanical properties of composite films. This result is consistent with that obtained by previous studies [45]. The graphene oxide quantum dots are combined into the cellulose membrane by ionic liquid. Hydrogen bonds are formed between the graphene peroxide quantum dots and the cellulose to form a strong bond, thus creating a stable composite membrane [46].

Table 4: Mechanical properties of active inner film of orange peel essential oil

Material	TS（MPa）	EB（%）	Thickness（μm）
PCH-0EOM	16.88±0.62c	40.20±1.20e	171.50±0.75e
PCH-10EOM	19.00±0.65bc	53.37±1.14d	176.60±1.11d
PCH-20EOM	20.95±0.50ab	55.60±0.96c	180.90±0.20c
PCH-30EOM	22.23±1.99a	68.37±1.01b	183.33±0.86b
PCH-40EOM	16.77±1.90c	75.47±0.81a	186.13±0.25a

To maximize the tensile strength (TS), PCH-30EOM and EC-20Zn/CD were compounded into a bilayer film (PCM@ECD). It can be seen from Table 6 that the thickness of the bilayer film is larger than that of the monolayer film, because this film was fabricated by sequentially layering thin films [via solution casting/spin-coating], followed by interfacial crosslinking. The thicker bilayer film enhances the mechanical properties (tensile strength, elongation at break). This enhancement may be attributed to hydrogen bonding between polymer chains and functional molecules (e.g. -OH/-NH groups), leading to densified crosslinking networks, which helps to improve the mechanical strength [47]. Gelatin-polyvinyl alcohol-carbon dot layer + corn starch-polyvinyl alcohol-cinnamon essential oil layer active bilayer film prepared by 3D printing technology has similar results [42].

Table 5: Mechanical Properties of Zn-CD Active Outer Film

Material	TS（MPa）	EB（%）	Thickness（μm）
EC-0Zn/CD	12.85±0.75cd	26.73±0.50c	162.5±0.72c
EC-10Zn/CD	17.82±1.51b	28.5±1.65c	165.67±2.05b
EC-20Zn/CD	23.27±0.99a	38.5±1.18b	168.7±2.62a
EC-30Zn/CD	15.27±3.92bc	36.43±0.67b	169.23±0.61a
EC-40Zn/CD	11.19±1.73d	44.33±2.83a	170.47±0.31a

Table 6: Mechanical Properties of Inner Film, Outer Film and Double Film

Material	TS（MPa）	EB（%）	Thickness（μm）
PCH-30EOM	22.23±1.99b	68.37±1.01b	183.33±0.86b
EC-20Zn/CD	23.27±0.99b	38.5±1.18c	168.7±2.62c
PCM-ECD	26.05±0.55a	71.93±0.45a	198.91±0.16a

DOI: 10.3844/ajbbsp.2026.22.01.006

As shown in Table 6, the tensile strength of the PCM@ECD double-layer film (28.7±1.2 MPa) was 87.6% higher than that of the single-layer PC film (15.3±0.8 MPa) ($p<0.01$) and was significantly higher than that of the pure EC film (22.1±1.0 MPa). Although the elongation at break (12.4±0.5%) was slightly lower than that of PC film (18.2±0.7%), it still met the flexibility requirements for packaging high-moisture food (>10%). This indicates that the incorporation of Zn-CD enhances the rigidity of the EC layer through crosslinking, while the PC microcapsule layer maintains the ductility of the film.

Surface Color and Optical Properties of Films

Table 7: Surface color of active inner film of orange peel essential oil microcapsule

Material	L*	a*	b*	ΔE*
PCH-0EOM	90.32±0.11a	0.15±0.01a	4.43±0.22e	5.73±0.18e
PCH-10EOM	89.37±0.10b	-0.12±0.01b	5.45±0.37d	7.02±0.21d
PCH-20EOM	88.47±0.26c	-0.15±0.02c	6.63±0.13c	8.39±0.16c
PCH-30EOM	87.01±0.13d	-0.22±0.01d	7.23±0.06b	9.94±0.15b
PCH-40EOM	86.29±0.13e	-0.33±0.03e	8.44±0.10a	11.2±0.16a

The surface color of the film is an important factor in evaluating the characteristics of the cling film, mainly due to its impact on the overall acceptability of the consumer [48]. The color change of the active inner layer film of orange peel essential oil is shown in Table 7. With the increase of EOM concentration, the brightness of the film decreases from 90.32 to 86.29, and the film color becomes dark (L* decreases), green (a * decreases) and yellow (b* increases). A similar change in color was observed in a study of antifungal films prepared with corn starch loaded orange essential oil [49]. The color change of the Zn-CD active outer layer film is shown in Table 8. As the Zn-CD content increases, the brightness of the film decreases from 96.20 to 91.67, the color of the film darkens (L* decreases), and carbon dots impart a red hue to the film (a* value moves positively) and yellow (b* increases). In a study of composite films prepared with carrageenan supported Zn-CD, the color of the films showed similar changes [44]. The brightness of the bilayer film is 86.7±0.50, which is acceptable, and Δ E* is less than that of most reported films, which has the potential for practical application.

Table 8: Surface color of Zn-CD active outer layer film

Material	L*	a*	b*	ΔE*
EC-0Zn/CD	96.20±0.27a	-1.27±0.12e	2.71±0.57e	1.30±0.18e
EC-10Zn/CD	95.46±0.08b	0.12±0.01d	5.37±0.19d	3.31±0.15d
EC-20Zn/CD	93.44±0.29c	0.25±0.02c	7.68±0.20c	5.76±0.24c
EC-30Zn/CD	92.41±0.34d	0.54±0.03b	8.42±0.34b	6.74±0.37b
EC-40Zn/CD	91.67±0.22e	0.78±0.01a	9.4±0.08a	7.83±0.03a

As shown in Table 9, the addition of a 0.01% Zn-CD EC layer increased the total color difference ΔE of the bilayer film to 10.78±0.19, which was within the distinguishable range of the naked eye (ΔE>5). Specifically, the b* value increased to 8.54±0.05, indicating a significant increase in the yellowing degree of the film surface ($p<0.05$), which was related to the fluorescence characteristics of Zn-CD. Despite this, the light transmittance (Fig. 11) of the film in the visible light region (600 nm) still reached 82.4±1.5%, which was only 8.1% lower than that of the control group (89.7±1.2%), confirming its limited impact on the visibility of packaging.

Table 9: Surface color of film, bilayer film

Material	L*	a*	b*	ΔE*
PCH-30EOM	87.0±0.13b	-0.2±0.01c	7.23±0.06c	9.94±0.15b
EC-20Zn/CD	93.4±0.29a	0.25±0.02a	7.68±0.2b	5.76±0.24c
PCM@ECD	86.7±0.50b	0.02±0.01b	8.54±0.05a	10.78±0.19a

The transmittance curve is shown in Fig. 11. With the increase of wavelength, the transmittance of EC-0Zn-CD gradually increases, and the transmittance reflects the transparency of the film, that is, the greater the transmittance, the higher the transparency. EC-0Zn-CD films exhibit the highest transmittance in the visible range (400~800 nm), which is attributed to their stable chemical properties. Because Zn-CD has ultraviolet absorption ability near 280nm, when ultraviolet light irradiates on

DOI: 10.3844/ajbbsp.2026.22.01.006

the film, Zn-CD can absorb this part of ultraviolet light and convert it into other forms of energy. Therefore, the introduction of Zn-CD endows the film with unique ultraviolet resistance. With the increase of Zn-CD concentration (EC-10Zn-CD to EC-30Zn-CD), the transmittance of films decreased significantly, which was mainly attributed to the enhancement of light scattering induced by Zn-CDs aggregation at high concentration and the indirect light absorption effect caused by surface hydroxyl vibration [40]. However, the existence of Zn-CD in the film still provides it with UV resistance, but the aggregation problem at high concentration affects its transmission performance in the visible range. in contrast, PCH-30EOM film had intermediate transmittance due to that fact that the size of orange peel essential oil microcapsule was much larger than visible wavelength, resulting in enhanced Mie scattering, but the network structure of chitosan-pectin matrix may partially limit microcapsule movement and reduce large size aggregate formation. In addition, carboxyl groups in pectin and amino groups in chitosan form hydrogen bond network, which enhances matrix continuity and partially offsets light scattering introduced by microcapsules. It is worth noting that the light transmittance of the PCM@ECD bilayer film is the lowest, and the light transmittance of the bilayer film decreases. This may be due to the absorption of light by surface functional groups in Zn-CD or the light scattering effect at the droplet interface. Light blocking caused. Although Zn-CD affects the transmittance, its surface functional groups absorb light in the ultraviolet region, which can improve the UV resistance of the film, so that the double-layer structure also enhances the UV blocking ability of the film to a certain extent [50].

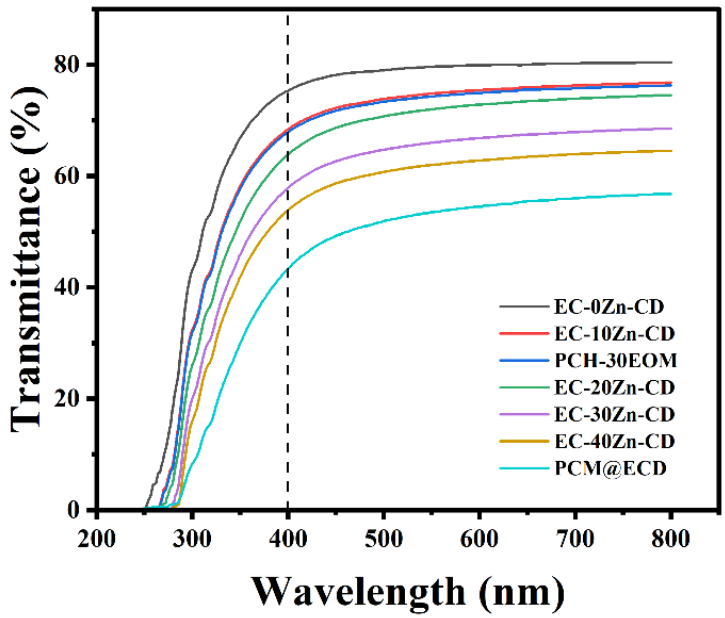

Fig. 11: Transmittance of film

Water Solubility of Films

The water resistance of film determines its applicability in food packaging with high water content, and water solubility is an important index to measure water resistance [51]. The experimental results are shown in Fig. 12. (A). With the increase of EOM concentration, the water solubility of the inner composite film decreases significantly ($p < 0.05$). The water solubility of pure chitosan pectin film can reach 24.22%. When 40 ml EOM is added, the water solubility of the film decreases to 12.91%. This may be because the interaction between OPEO microcapsules and the matrix of composite film hinders the strong hydrogen bond interaction between matrix and water molecules [25]. A recent study reported similar findings, with the addition of chitosan-encapsulated thyme essential oil microcapsules to potato starch-pectin composite films significantly reducing water solubility compared to controls [31]. The water solubility of the outer films increased with the increase of Zn-CD content. Pure ethyl cellulose film is insoluble in water. When 40 mg Zn-CD is added, the water solubility of the film increases to 0.61%. This may be because the number of hydrophilic functional groups increases with the addition of Zn-CD, resulting in an increase in the solubility of the film [5]. In a previous study, glucose was used as carbon source and nitrogen as functional group. Carbon dots prepared by hydrothermal method were added to cellulose nanofiber based composite films. Due to the hydrophilicity of carbon dots, the water solubility of the films was increased [52]. Through physical adsorption between the two layers, the overall water solubility is close to the superposition of two layers.

DOI: 10.3844/ajbbsp.2026.22.01.006

Water Vapor Permeability of Thin Films

Water vapor permeability is considered to be an important indicator for evaluating the performance of packaging films. High water vapor barrier ability is conducive to limiting the migration of water molecules, thus prolonging the shelf life of foods. The smaller water vapor permeability, the better the ability of the film to block water vapor [53]. The obtained packaging material with good water vapor barrier ability can prevent moisture loss of packaged foods such as fresh vegetables, fruits, and meat thereby achieving better preservation effect. As shown in Fig. 12. (B), the WVP of the inner layer film decreased first and then increased as the amounts of microcapsules added increased. The WVP of the inner layer film without adding microcapsules was 1.78×10^{-12}g·cm/s·cm^2·Pa, and when 30ml of microcapsules were added, the WVP decreased to 0.95×10^{-12}g·cm/s·cm^2·Pa, and the WVP of the inner layer film increased to 1.11×10^{-12}g·cm/s·cm^2·Pa by continuing to add microcapsules. This is because adding a proper number of microcapsules makes them evenly distributed in the membrane, filling the gaps between the membranes, making the membrane structure denser and water vapor more difficult to pass through. The water vapor transmission coefficient increases with the increase of microcapsule addition amount, which is due to the excessive addition of microcapsules, uneven dispersion, resulting in agglomeration, agglomeration leads to the destruction of the structure of chitosan pectin film and the appearance of cracks, thus increasing the water vapor transmission coefficient.

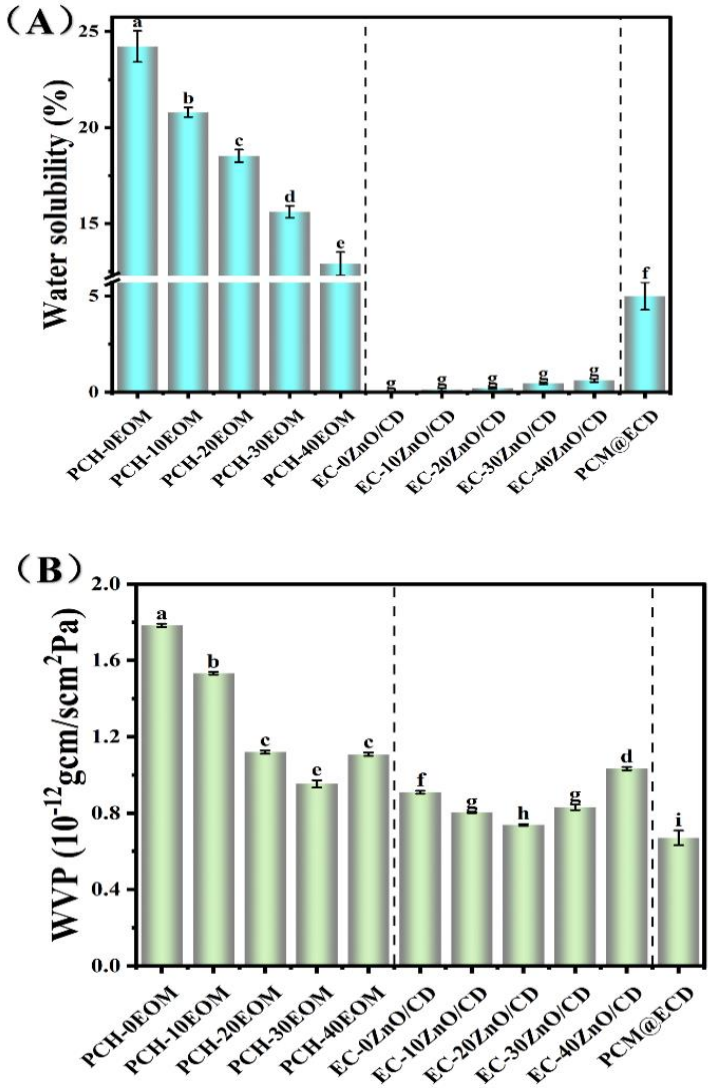

Fig. 12: (A) Water solubility of film;(B) Water vapor permeability of film

Similar results were observed in a previous study of corn starch polylactic acid composite bilayer films with eucalyptus essential oil microcapsules [54]. The WVP of the outer film decreased firstly and then increased with the addition of Zn-CD. The WVP of the inner film without Zn-CD was 0.91×10^{-12}g·cm/s·cm^2·Pa, and decreased to 0.74×10^{-12}g·cm/s·cm^2·Pa with the addition of 20mg microcapsules. This may be due to the hydrogen bond interaction between Zn-CD and the film matrix, which reduced the free volume of the film matrix macromolecules and increased the difficulty of water molecules penetrating the film [55]. The WVP of the outer film increases to 1.03×10^{-12}g·cm/s·cm^2·Pa with the addition of Zn-CD, which may be due to the existence of a large number of hydroxyl groups in Zn-CD and the increase of surface roughness and water vapor permeability caused by the aggregation of carbon dots [5]. The bilayer film has a stronger water vapor barrier capacity WVP as low as 0.67×10^{-12}g·cm/s·cm^2·Pa , which can be attributed to its larger overall film thickness, which prevents the diffusion of water molecules in the film, thus further making the bilayer film have a higher overall water vapor barrier capacity [42] (Chen et al. 2024). The PCM@ECD bilayer films prepared in this study have better water vapor barrier capacity than many reported bilayer biopolymer films. For example, the WVP of the double-layer packaging film prepared by glutenin/tamarind gelatin-loaded melatonin/grapefruit essential oil binary microemulsion is 6.252gmm/dm^{2}KPa. The WVP of the PLA/ tilapia gelatin-sodium alginate billet film prepared by coating method, which was supported with cinnamaldehyde and thyme phenol complexes, were 9.16×10^{-11}g/msPa and 9.38×10^{-11}g/msPa [56]. The WVP of chitosan/agarose films were 0.85 g·mm/m²·h·kPa, and those of glutaraldehyde gelatin-gelatin composite films were 0.52 g·mm/m²·h·kPa, WVP of whey protein-MRP encapsulated films were 0.48 g·mm/m²·h·kPa [5, 6, 31]. The superior moisture barrier is attributed to the hydrophobic Ethyl Cellulose (EC) outer layer effectively inhibiting water penetration [31].

Bacteriostatic Ability of Films

Shewanella putrefaciens and *Pseudomonas* sp., the dominant putrefactive bacteria of salmon, were studied. The growth curve of bacteria in 24 h was determined to study the antibacterial performance of the film. As shown in Fig. 13. (A) and (B), untreated Shewanella putrefaciens and Pseudomonas grew faster as the incubation time increased. For PCH treatment group, Fig. 13. (A) shows that the growth curves almost overlap with those of control group, and the membrane itself has no significant bacteriostasis against Shewanella putrefaciens, which may be due to the fact that although chitosan has antibacterial properties, the hydrophilicity of pectin weakens the physical barrier effect of membrane against hydrophobic pathogens. Fig. 13. (B) shows that the composite membrane slightly promotes Pseudomonas growth (OD_{600} increases by 3%), probably because membrane degradation products such as oligosaccharides can be utilized as carbon sources [57] (Zhuang et al. 2024). For the PCH-EOM treated group, Fig. 13. (A) and (B) show that the addition of essential oils is significant ($p < 0.05$) enhanced the membrane's antibacterial ability against Shevaleria putreformis and Pseudomonas. This might be due to the fact that the main active component of orange peel essential oil is limonene, which penetrates the cell membrane and increases membrane permeability, leading to intracellular ATP leakage [58] (Abdul-Rahaman et al. 2025). The antibacterial rate against Shevaleria putreformis reached 73.2%. However, the inhibition rate against Pseudomonas was only 39.4%. This may be because the outer membrane Lipopolysaccharide (LPS) of Pseudomonas was dense and had AcrAB-TolC efflux pump [57]. Can actively discharge antibacterial molecules, directly add essential oil film takes effect quickly but volatile [57]. For EOM film treatment group, the greater the addition amount, the stronger the inhibition. Meanwhile, due to slow release, the inhibition was not obvious in the initial stage, but obvious in the later stage. Fig.13. (B) shows that the inhibition effect of 10ml and 20ml microcapsule groups was insufficient, and the biomass in the later stage exceeded that of the control group.

This may be because Pseudomonas had adaptability to low concentration of essential oil, and higher concentration was needed to achieve significant inhibition on Pseudomonas. The inhibition rate of 40ml microcapsule film against Shewanella putrefaciens was 94.2% and Pseudomonas sp. was 63.6%, but the mechanical properties of the film decreased because of microcapsule aggregation. The inhibition rate of Shewanella putrefaciens was increased from 73.2%(PCH) to 78.3%(PCH-30EOM) when treated with 30 ml microcapsules, but the inhibition rate against Pseudomonas was only 30.3%. For PCM@ECD double-layer membrane treatment group, due to the synergistic effect of slow release of double-layer membrane and carbon dots, the bacteriostatic effect was enhanced, the growth curve was smoother, the bacteriostatic rate against Shewanella putrefaciens increased to 87.0%, and the bacteriostatic rate against Pseudomonas increased to 66.7%, which may be due to the hydrophobicity of ethyl cellulose reducing water vapor permeation, inhibiting bacterial mobility, and blocking quorum sensing signals.(AHLs such as Pseudomonas) [59], and ultra-small Zn-CDs with high positive charge characteristics can interact with bacterial membranes and destroy their integrity and can generate ROS under visible light. ROS show good antibacterial effect through oxidative damage to cellular DNA, RNA, proteins and lipids [60].

DOI: 10.3844/ajbbsp.2026.22.01.006

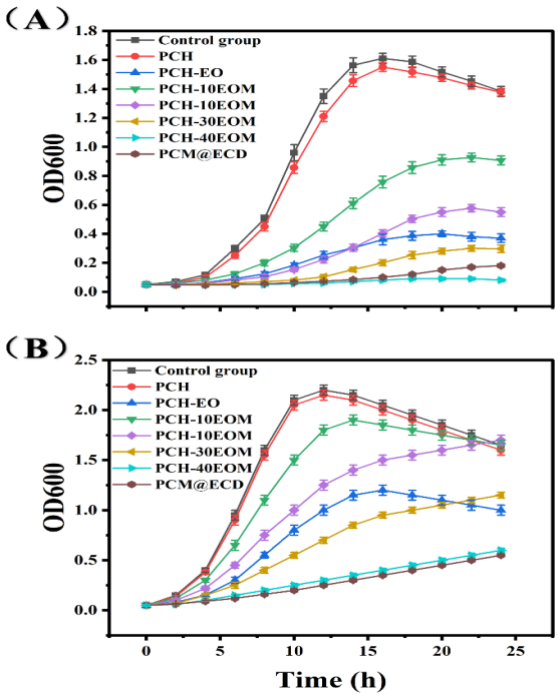

Fig. 13: Effect of film on growth curve of (A) Shewanella putrefaciens (B) Pseudomonassp.

Oxidation Resistance of Films

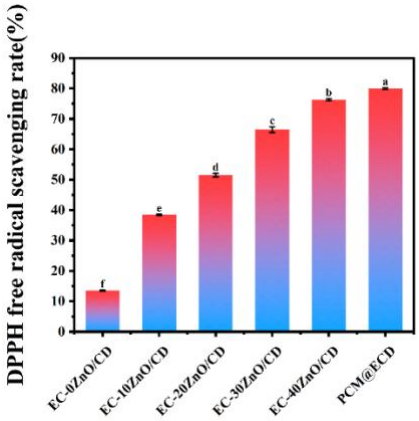

Fig. 14: Oxidation resistance of thin films

The use of suitable packaging films containing antioxidants neutralizes or removes harmful compounds released during food storage, such as free radical oxidants, and helps to extend the shelf life of packaged products [35] (Khan et al. 2023). The antioxidant activity of packaging film can inhibit lipid peroxidation of food, which is of great significance to the quality of food. DPPH method is considered to be one of the methods to determine the antioxidant activity of packaging film [61]. Therefore, we evaluated the antioxidant effect of the films by measuring their ability to scavenge DPPH free radicals. Ethyl Cellulose (EC), as hydrophobic matrix, lacks electron donor groups and depends mainly on physical barrier effect. Its DPPH clearance rate is low, which is 13.51%. Zn-CD is the main antioxidant of the films. The addition of Zn-CD significantly ($p < 0.05$) improves the antioxidant activity of the films and shows a concentration-dependent trend. When the addition of Zn-CD is 40mg, the DPPH radical scavenging rate of the outer films reaches 76.33%. This is due to the existence of a large number of phenolic groups in the active functional groups (such as hydroxyl and carboxyl) of Zn-CD, which scavenge free radicals and block free radical chain reactions [62]. The DPPH radical scavenging rate of PCM@ECD bilayer membrane reached 79.97%, which may be due to the synergistic mechanism of bilayer membrane. Hesperidin (flavonoids) and limonene (terpenes), the main active components of orange peel essential oil, provide phenolic hydroxyl groups, donate electrons

directly [63], and hydrophobic ethyl cellulose reduces the dissolution of antioxidants. The DPPH radical scavenging rate of this film is higher than that of most carbon dot films. For example, the DPPH radical scavenging rate of polyvinyl alcohol (PVA)/Corn Starch (CS) composite film loaded with pitaya carbon dots prepared by Liu, Zhenbin, et al. is 45.61% [45] (Liu et al. 2024). The DPPH free radical scavenging rate of chitosan/gelatin film loaded banana peel carbon point was 74.5% [64]. The results show that the composite film has good antioxidant properties and is suitable for active packaging of high fat foods.

Conclusion

In this study, the improvement of OPEOM embedding rate is attributed to the orthogonal design's analysis of interaction. Although single-factor experiments showed that the encapsulation rate was the highest at pH 4.5 (79.56%), when the chitosan concentration increased to 0.30% w/v (B_3), pH 4.0 (A_1) * formed a denser coagulation network by enhancing the electrostatic attraction between chitosan proproton ($+NH_3^+$) and pectin carboxyl ($-COO^-$) (SEM Figure 4c). This is consistent with the conclusion reported by [6] Park et al. (2022) that "reducing pH at polymer concentration can inhibit phase separation". In addition, an OPEO concentration of 0.70% w/v (C_2) balanced core material release and wall material stability, while 30 min (D_2) ensured adequate crosslinking and prevented TG enzyme inactivation. The addition of orange peel essential oil microcapsules and zinc-doped carbon dots effectively improved the film-forming performance of the inner and outer layers. The optimal addition amounts of orange peel essential oil microcapsules and zinc-doped carbon dots were 30ml and 20mg respectively, that is, 15% (v/v) and 0.01% (w/v). The optimal process conditions for preparing orange peel essential oil microcapsules by the complex coagulation method are as follows: pH4.0, chitosan concentration 0.3%, orange peel essential oil concentration 0.7%, and reaction time 30 min. The maximum embedding rate of the obtained orange peel essential oil microcapsules is (83.08±0.51) %. The average particle size of Zn-CD prepared by the hydrothermal synthesis method was 1.72 nm. The active bilayer (PCM@ECD) with Pectin - Chitosan Composite (PC) and Ethyl Cellulose (EC) as the membrane matrix and Orange Peel Essential Oil Microcapsules (OPEOM) and Zn-CD as the active components of the inner and outer layers of the membrane, was prepared by the continuation flow method and layer self-assembly technique. It has good water resistance, UV blocking ability, antibacterial and antioxidant activity. Among them, OPEOM mainly provided antibacterial function, with an inhibition rate of 87.0% against *Shivonas putrefaction* and 66.7% against *Pseudomonas aeruginosa*. Zn-CD mainly provided UV blocking and antioxidant function, and the free radical scavenging rate of DPPH in PCM@ECD bilayers reached 79.97%. Hence, this study highlights the important role of PCM@ECD in food preservation.

Acknowledgment

First of all, we would like to express our gratitude to the publisher for its support in publishing this research article. Secondly, we would like to express our gratitude to the editorial team for their efforts in reviewing and editing our work. Finally, we are grateful for the opportunity to contribute to the field of research through this publication.

Funding Information

This research was supported by the National Natural Science Foundation of China Project (U22A20542).

Author’s Contributions

Yan Zhao: Original draft preparation, methodology, investigation, data analysis.

Heng Zhang: Investigation, data analysis, supervision.

Yanfei Zhao: Investigation, data analysis, supervision.

Madiha Younas: Article layout, polishing.

Qingfeng Rong: Investigation, Data analysis.

Qing Shao: Investigation, data analysis.

Lanlan Zhu: Writing and editing, supervision, project management, and fund acquisition.

Ethics

This article and the unpublished materials are original. The corresponding author confirms that all other authors have read and approved the manuscript, and there are no ethical issues.

References

1. Zou, Y., J. Ren, Y. Fan, Y. Cao, Y. Xie, X. Xiao, and F. Liu. 2025. Enhanced hydrophobicity, antioxidant activity, and antimicrobial efficacy of edible starch-based films incorporating pullulan and geraniol for fresh salmon preservation. *Food Packaging and Shelf Life* 49: 101530. doi: 10.1016/j.fpsl.2025.101530.
2. Yu, D., J. M. Regenstein, and W. Xia. 2019. Bio-based edible coatings for the preservation of fishery products: A Review. *Critical Reviews in Food Science and Nutrition* 59(15): 2481–2493. doi: 10.1080/10408398.2018.1457623.
3. de Paiva, E. L., R. F. Milani, B. S. Boer, K. D. Quintaes, and M. A. Morgano. 2017. Methylmercury in fish species used in preparing *sashimi*: A case study in Brazil. *Food Control* 80: 104–112. doi: 10.1016/j.foodcont.2017.04.027.
4. Kim, Y. H., Kim, H.-J., Yoon, K. S., & Rhim, J.-W. (2023). Cellulose nanofiber/deacetylated quaternary chitosan composite packaging film for growth inhibition of Listeria monocytogenes in raw salmon. *Food Packaging and Shelf Life, 35*, 101040.
5. Khoshkalampour, A., M. Ghorbani, and Z. Ghasempour. 2023. Cross-linked gelatin film enriched with green carbon quantum dots for bioactive food packaging. *Food Chemistry* 404: 134742. doi: 10.1016/j.foodchem.2022.134742.
6. Park, K. J., Lee, J.-S., Jo, H. J., Kim, E. S., & Lee, H. G. (2022). Antimicrobial and indicator properties of edible film containing clove bud oil-loaded chitosan capsules and red cabbage for fish preservation. *International Journal of Biological Macromolecules, 196*, 163-171.
7. Magalhães, M. L., M. Ionta, G. Á. Ferreira, M. L. L. Campidelli, D. L. Nelson, V. R. F. Ferreira, D. A. D. C. S. Rezende, and M. D. G. Cardoso. 2020. Biological activities of the essential oil from the Moro orange peel (*Citrus sinensis* (L.) Osbeck). *Flavour and Fragrance Journal* 35(3): 294–301. doi: 10.1002/ffj.3561.
8. Razola-Díaz, M. del C., E. J. Guerra-Hernández, B. García-Villanova, and V. Verardo. 2021. Recent developments in extraction and encapsulation techniques of orange essential oil. *Food Chemistry* 354: 129575. doi: 10.1016/j.foodchem.2021.129575.
9. Li, Y., C. Wu, T. Wu, L. Wang, S. Chen, T. Ding, and Y. Hu. 2018. Preparation and characterization of citrus essential oils loaded in chitosan microcapsules by using different emulsifiers. *Journal of Food Engineering* 217: 108–114. doi: 10.1016/j.jfoodeng.2017.08.026.
10. Jun-xia, X., Y. Hai-yan, and Y. Jian. 2011. Microencapsulation of sweet orange oil by complex coacervation with soybean protein isolate/gum Arabic. *Food Chemistry* 125(4): 1267–1272. doi: 10.1016/j.foodchem.2010.10.063.
11. Feng, L., N. Zhang, J. Wang, X. Jiang, J. Han, L. Li, H. Kitazawa, X. Wang, C. Chen, and Y. Guo. 2024. Sustained release of a novel bilayer packaging film loaded with binary microemulsion of melatonin/pummelo essential oil and its regulation of postharvest energy metabolism in *Agaricus bisporus*. *Food Control* 161: 110396. doi: 10.1016/j.foodcont.2024.110396.
12. Wang, K.-L., Yu, B.-K., Zhao, H.-F., Liu, Y.-X., Wu, C.-Y., Zhang, Y.-H., & Mu, Z.-S. (2025). Preparation and characterization of microcapsules for tuna oil by maillard reaction products of whey protein isolate and Arabic gum via complex coacervation. *Food Chemistry*, 143269.
13. Abdalla, G., C. U. Mussagy, G. Sant'Ana Pegorin Brasil, M. Scontri, J. C. da Silva Sasaki, Y. Su, C. Bebber, R. R. Rocha, A. P. de Sousa Abreu, R. P. Goncalves, B. S. Burd, M. F. Pacheco, K. M. Romeira, F. P. Picheli, N. B. Guerra, N. Farhadi, J. F. Floriano, S. Forster, S. He, H. T. Nguyen, A. Peirsman, Z. Tirpáková, S. Huang, M. R. Dokmeci, E. S. Ferreira, L. S. dos Santos, R. D. Piazza, R. F. C. Marques, A. Goméz, G. R. Silva, V. Jucaud, B. Li, H. M. C. de Azeredo, and R. D. Herculano. 2023. Eco-sustainable coatings based on chitosan, pectin, and lemon essential oil nanoemulsion and their effect on strawberry preservation. *International Journal of Biological Macromolecules* 249: 126016. doi: 10.1016/j.ijbiomac.2023.126016.
14. Akhter, R., F. A. Masoodi, and T. A. Wani. 2024. Chitosan, gelatin and pectin based bionanocomposite films with rosemary essential oil as an active ingredient for future foods. *International Journal of Biological Macromolecules* 272: 132813. doi: 10.1016/j.ijbiomac.2024.132813.
15. Tang, Y., X. Zhang, R. Zhao, D. Guo, and J. Zhang. 2018. Preparation and properties of chitosan/guar gum/nanocrystalline cellulose nanocomposite films. *Carbohydrate Polymers* 197: 128–136. doi: 10.1016/j.carbpol.2018.05.073.
16. Sharaby, M. R., E. A. Soliman, A. B. Abdel-Rahman, A. Osman, and R. Khalil. 2022. Novel pectin-based nanocomposite film for active food packaging applications. *Scientific Reports* 12(1): 20673. doi: 10.1038/s41598-022-25192-4.
17. Zhao, L., M. Zhang, A. S. Mujumdar, B. Adhikari, and H. Wang. 2022. Preparation of a Novel Carbon Dot/Polyvinyl Alcohol Composite Film and Its Application in Food Preservation. *ACS Applied Materials & Interfaces* 14(33). American Chemical Society: 37528–37539. doi: 10.1021/acsami.2c10869.
18. Zhao, L., M. Zhang, A. S. Mujumdar, and H. Wang. 2023. Application of carbon dots in food preservation: a critical review for packaging enhancers and food preservatives. *Critical Reviews in Food Science and Nutrition* 63(24): 6738–6756. doi: 10.1080/10408398.2022.2039896.
19. Jayakumar, A., S. Radoor, G. H. Shin, and J. T. Kim. 2024. Lemon peel-based fluorescent carbon quantum dots as a functional filler in polyvinyl alcohol-based films for active packaging applications. *Industrial Crops and Products* 209: 117968. doi: 10.1016/j.indcrop.2023.117968.
20. Jiang, Z., J. Feng, Y. Dai, W. Yu, S. Bai, C. Bai, Z. Tu, P. Guo, T. Liao, and L. Qiu. 2025. Preparation of a biodegradable packaging film by konjac glucomannan/sodium alginate reinforced with nitrogen-doped carbon quantum dots from crayfish shell for crayfish meat preservation. *International Journal of Biological Macromolecules* 297: 139596. doi: 10.1016/j.ijbiomac.2025.139596.
21. Cai, M., X. Zhang, H. Zhong, C. Li, C. Shi, H. Cui, and L. Lin. 2024. Ethyl cellulose/gelatin-carboxymethyl chitosan bilayer films doped with *Euryale ferox* seed shell polyphenol for cooked meat preservation. *International Journal of Biological Macromolecules* 256: 128286. doi: 10.1016/j.ijbiomac.2023.128286.

22. Qian, J., Y. Chen, Q. Wang, X. Zhao, H. Yang, F. Gong, and H. Guo. 2021. Preparation and antimicrobial activity of pectin-chitosan embedding nisin microcapsules. *European Polymer Journal* 157: 110676. doi: 10.1016/j.eurpolymj.2021.110676.
23. Khan, A., Z. Riahi, J. Tae Kim, and J.-W. Rhim. 2024. Carrageenan-based multifunctional packaging films containing Zn-carbon dots/anthocyanin derived from Kohlrabi peel for monitoring quality and extending the shelf life of shrimps. *Food Chemistry* 432: 137215. doi: 10.1016/j.foodchem.2023.137215.
24. Wu, H., X. Du, X. Guo, J. Cai, H. Chen, C. Chen, Y. Shi, Y. Zhang, X. Pan, X. Guan, and L. Zhang. 2025. Chitosan-based Pickering double emulsion microcapsules improve the UV stability and the persistence of *Bacillus thuringiensis* on mosquito control. *Carbohydrate Polymers* 354: 123346. doi: 10.1016/j.carbpol.2025.123346.
25. Wang, W., W. Zhang, L. Li, W. Deng, M. Liu, and J. Hu. 2023. Biodegradable starch-based packaging films incorporated with polyurethane-encapsulated essential-oil microcapsules for sustained food preservation. *International Journal of Biological Macromolecules* 235: 123889. doi: 10.1016/j.ijbiomac.2023.123889.
26. Gao, M., M. Ji, Y. He, X. Pan, Y. Wang, T. Si, and Y. Sun. 2023. Construction of consumer-friendly essential oil microcapsules with viscous cores to provide extra long-lasting release. *Powder Technology* 413: 118040. doi: 10.1016/j.powtec.2022.118040.
27. Wan, Y., Z. Niu, X. Luo, W. Jin, Z. Liu, C. Wei, and W. Liu. 2024. Insights on tiger nut (*Cyperus Esculentus* L.) oil-loaded microcapsules: characterization and oxidation stability analysis. *Food Chemistry* 460: 140755. doi: 10.1016/j.foodchem.2024.140755.
28. Qiu, L., M. Zhang, B. Adhikari, and L. Chang. 2022. Microencapsulation of rose essential oil in mung bean protein isolate-apricot peel pectin complex coacervates and characterization of microcapsules. *Food Hydrocolloids* 124: 107366. doi: 10.1016/j.foodhyd.2021.107366.
29. Zhong, X., M. Zhang, C. L. Law, and Y. Liu. 2025. Foam-based mustard essential oil microcapsules preparation, characterization, grilling application and comparison with emulsion microcapsules. *Food Chemistry* 478: 143758. doi: 10.1016/j.foodchem.2025.143758.
30. Cui, F., R. Fan, D. Wang, L. Ren, Q. Wang, Y. Meng, R. Ma, S. Wang, Z. Liu, X. Li, T. Li, and J. Li. 2024. Super Fe3+ competing ability, high biocompatibility, and mild antibacterial carbon dots for food preservation. *Chemical Engineering Journal* 492: 152103. doi: 10.1016/j.cej.2024.152103.
31. Wang, J., L. Li, Y. Li, Q. Song, Y. Hu, Q. Wang, and S. Lu. 2025. Characterization of thyme essential oil microcapsules and potato starch/pectin composite films
32. Lu, W., X. Qin, S. Liu, G. Chang, Y. Zhang, Y. Luo, A. M. Asiri, A. O. Al-Youbi, and X. Sun. 2012. Economical, Green Synthesis of Fluorescent Carbon Nanoparticles and Their Use as Probes for Sensitive and Selective Detection of Mercury(II) Ions. *Analytical Chemistry* 84(12): 5351–5357. doi: 10.1021/ac3007939.
33. Li, Y., C. Ma, J. Ma, W. Guo, Y. Liu, Z. Jing, Z. Wang, L. Feng, W. Zhang, and Q. Xu. 2021. Promoting potential direct interspecies electron transfer (DIET) and methanogenesis with nitrogen and zinc doped carbon quantum dots. *Journal of Hazardous Materials* 410: 124886. doi: 10.1016/j.jhazmat.2020.124886.
34. Hu, F., Q. Fu, Y. Li, C. Yan, D. Xiao, P. Ju, Z. Hu, H. Li, and S. Ai. 2024. Zinc-doped carbon quantum dots-based ratiometric fluorescence probe for rapid, specific, and visual determination of tetracycline hydrochloride. *Food Chemistry* 431: 137097. doi: 10.1016/j.foodchem.2023.137097.
35. Khan, A., P. Ezati, and J.-W. Rhim. 2023a. Chitosan/gelatin-based multifunctional film integrated with green tea carbon dots to extend the shelf life of pork. *Food Packaging and Shelf Life* 37: 101075. doi: 10.1016/j.fpsl.2023.101075.
36. Dong, Y., H. Pang, H. B. Yang, C. Guo, J. Shao, Y. Chi, C. M. Li, and T. Yu. 2013. Carbon-Based Dots Co-doped with Nitrogen and Sulfur for High Quantum Yield and Excitation-Independent Emission. *Angewandte Chemie International Edition* 52(30): 7800–7804. doi: 10.1002/anie.201301114.
37. Bu, N., N. Zhou, G. Cao, R. Mu, J. Pang, C. Ma, and L. Wang. 2023. Konjac glucomannan/carboxymethyl chitosan film embedding gliadin/casein nanoparticles for grape preservation. *International Journal of Biological Macromolecules* 249: 126131. doi: 10.1016/j.ijbiomac.2023.126131.
38. Ye, Y., F. Zeng, M. Zhang, S. Zheng, J. Li, and P. Fei. 2020. Hydrophobic edible composite packaging membrane based on low-methoxyl pectin/chitosan: Effects of lotus leaf cutin. *Food Packaging and Shelf Life* 26: 100592. doi: 10.1016/j.fpsl.2020.100592.
39. Cao, D., Q. Li, X. Sun, Y. Wang, X. Zhao, E. Cakmak, W. Liang, A. Anderson, S. Ozcan, and H. Zhu. 2021. Amphipathic Binder Integrating Ultrathin and Highly Ion-Conductive Sulfide Membrane for Cell-Level High-Energy-Density All-Solid-State Batteries. *Advanced Materials* 33(52): 2105505. doi: 10.1002/adma.202105505.
40. Li, T., F. Meng, W. Chi, S. Xu, and L. Wang. 2022. An Edible and Quick-Dissolving Film from Cassia Gum and Ethyl Cellulose with Improved Moisture Barrier for Packaging Dried Vegetables. *Polymers* 14(19): 4035. doi: 10.3390/polym14194035.
41. Baghi, F., A. Gharsallaoui, E. Dumas, G. Agusti, and S. Ghnimi. 2024. Characterization of antimicrobial multilayer film based on ethylcellulose-pectin incorporated with nanoemulsions of *trans*-cinnamaldehyde essential oil. *Food Chemistry: X* 22: 101261. doi: 10.1016/j.fochx.2024.101261.
42. Chen, K., M. Zhang, B. Bhandari, and D. Deng. 2024. 3D printed cinnamon essential oil/banana peel carbon dots loaded corn starch/gelatin bilayer film with enhanced functionality for food packaging application. *Food Chemistry* 448: 139176. doi: 10.1016/j.foodchem.2024.139176.
43. Ebrahimzadeh, S., D. Biswas, S. Roy, and D. J. McClements. 2023. Incorporation of essential oils in edible seaweed-based films: A comprehensive review. *Trends in Food Science & Technology* 135: 43–56. doi: 10.1016/j.tifs.2023.03.015.
44. Zhang, L., W. Wang, Y. Ni, C. Yang, X. Jin, Y. Wang, Y. yang, Y. Jin, J. Sun, and J. Wang. 2022. ZnO/C-mediated k-carrageenan based pseudo-pasteurization films for kumquat preservation. *Food Hydrocolloids* 128: 107582. doi: 10.1016/j.foodhyd.2022.107582.
45. Liu, Z., M. Cui, R. Weng, H. E, H. Li, S. Hati, L. Hu, and H. Mo. 2024. Incorporation of carbon dots into polyvinyl alcohol/corn starch based film and its application on shiitake mushroom preservation. *International Journal of Biological Macromolecules* 280: 135998. doi: 10.1016/j.ijbiomac.2024.135998.
46. Colburn, A., N. Wanninayake, D. Y. Kim, and D. Bhattacharyya. 2018. Cellulose-graphene quantum dot composite membranes using ionic liquid. *Journal of Membrane Science* 556: 293–302. doi: 10.1016/j.memsci.2018.04.009.

47. Mou, L., W. Jiang, Y. Lu, J. Li, G. Li, H. Yuan, Z. Jiang, L. Zhang, and T. Ming. 2025. Strawberry preservation using multilayer chitosan films grafted with phenolic acids and loaded with γ-CD-MOFs encapsulated antifungal agents. *International Journal of Food Microbiology* 439: 111247. doi: 10.1016/j.ijfoodmicro.2025.111247.
48. Reichembach, L. H., P. Guerrero, C. L. de Oliveira Petkowicz, and K. de la Caba. 2024. Valorization of pectins from coffee wastes for the development of pectin-chitosan films. *Carbohydrate Polymers* 334: 122057. doi: 10.1016/j.carbpol.2024.122057.
49. do Evangelho, J. A., G. da Silva Dannenberg, B. Biduski, S. L. M. el Halal, D. H. Kringel, M. A. Gularte, A. M. Fiorentini, and E. da Rosa Zavareze. 2019. Antibacterial activity, optical, mechanical, and barrier properties of corn starch films containing orange essential oil. *Carbohydrate Polymers* 222: 114981. doi: 10.1016/j.carbpol.2019.114981.
50. Gong, X., Q. Xu, X. Chen, F. Meng, and H. Wang. 2023. Solvent-free rapid synthesis of carbon nanodots at atmospheric pressure: Preparation of transparent light conversion films with ultrahigh efficient UV and blue light shielding. *Carbon* 210: 118044. doi: 10.1016/j.carbon.2023.118044.
51. Li, X.-L., Y. Shen, F. Hu, X.-X. Zhang, K. Thakur, K. R. R. Rengasamy, M. R. Khan, R. Busquets, and Z.-J. Wei. 2023. Fortification of polysaccharide-based packaging films and coatings with essential oils: A review of their preparation and use in meat preservation. *International Journal of Biological Macromolecules* 242: 124767. doi: 10.1016/j.ijbiomac.2023.124767.
52. Ezati, P., J.-W. Rhim, R. Molaei, R. Priyadarshi, and S. Han. 2022. Cellulose nanofiber-based coating film integrated with nitrogen-functionalized carbon dots for active packaging applications of fresh fruit. *Postharvest Biology and Technology* 186: 111845. doi: 10.1016/j.postharvbio.2022.111845.
53. Jiang, J., P. S. M. S. L. Watowita, R. Chen, Y. Shi, J.-T. Geng, K. Takahashi, L. Li, and K. Osako. 2022. Multilayer gelatin/myofibrillar films containing clove essential oil: Properties, protein-phenolic interactions, and migration of active compounds. *Food Packaging and Shelf Life* 32: 100842. doi: 10.1016/j.fpsl.2022.100842.
54. Chen, M., X. Yan, M. Cheng, P. Zhao, Y. Wang, R. Zhang, X. Wang, J. Wang, and Mengmeng Chen. 2022. Preparation, characterization and application of poly(lactic acid)/corn starch/eucalyptus leaf essential oil microencapsulated active bilayer degradable film. *International Journal of Biological Macromolecules* 195: 264–273. doi: 10.1016/j.ijbiomac.2021.12.023.
55. Nie, X., Y. Gong, N. Wang, and X. Meng. 2015. Preparation and characterization of edible myofibrillar protein-based film incorporated with grape seed procyanidins and green tea polyphenol. *LWT - Food Science and Technology* 64(2): 1042–1046. doi: 10.1016/j.lwt.2015.07.006.
56. Chen, J., Y. Li, Y. Wang, S. Yakubu, H. Tang, and L. Li. 2022. Active polylactic acid/tilapia fish gelatin-sodium alginate bilayer films: Application in preservation of Japanese sea bass (*Lateolabrax japonicus*). *Food Packaging and Shelf Life* 33: 100915. doi: 10.1016/j.fpsl.2022.100915.
57. Zhuang, S., S. Liang, X. Xiong, and Y. Luo. 2024. Effect of Interactions Between Grass Carp Spoilage Bacteria *Pseudomonas putida* and *Shewanella putrefaciens* on Their Spoilage Potentials. *Journal of Food Science and Technology* 42(4): 156–163. doi: 10.12301/spxb202300426.
58. Abdul-Rahaman, A., S. V. Irtwange, K. P. Aloho, A. N. Yadav, and B. Barau. 2025. Pathogenicity and molecular characterization of bacteria isolates at postharvest storage of Ibadan sweet, Valencia, and Washington navel citrus fruits. *Vegetos*. doi: 10.1007/s42535-025-01303-0.
59. Yang, J., and X. Liu. 2025. A new type of cationic surfactant prepared by surface modification on sucrose carbon dots via an entirely green approach and the inhibition on growth of *E. coli* and *S. aureus*. *Carbohydrate Research* 554: 109541. doi: 10.1016/j.carres.2025.109541.
60. Li, F., Zhu, S., Du, Y., Zhe, T., Ma, K., Liu, M., & Wang, L. (2024). Carrageenan/polyvinyl alcohol composite film reinforced with spermidine carbon dots: An active packaging material with dual-mode antibacterial activity. *International Journal of Biological Macromolecules, 266*, 131343.
61. Deng, J., W. Cheng, and G. Yang. 2011. A novel antioxidant activity index (AAU) for natural products using the DPPH assay. *Food Chemistry* 125(4): 1430–1435. doi: 10.1016/j.foodchem.2010.10.031.
62. Khan, A., P. Ezati, and J.-W. Rhim. 2023b. Chitosan/gelatin-based multifunctional film integrated with green tea carbon dots to extend the shelf life of pork. *Food Packaging and Shelf Life* 37: 101075. doi: 10.1016/j.fpsl.2023.101075.
63. Ge, W., J. Chen, Y. Wang, Z. Hu, and H. Wang. 2025. Insight on the functionalization of hesperidin: Encapsulated by the complex of soybean protein isolate and polysaccharides. *Food Chemistry* 488: 144902. doi: 10.1016/j.foodchem.2025.144902.
64. Sul, Y., Ezati, P., & Rhim, J.-W. (2023). Preparation of chitosan/gelatin-based functional films integrated with carbon dots from banana peel for active packaging application. *International Journal of Biological Macromolecules, 246*, 125600. and their impact on the quality of chilled mutton. *Food Chemistry* 464: 141692. doi: 10.1016/j.foodchem.2024.141692.